On the importance of plant phenology in the evaporative process of a semi-arid woodland: Could it be why satellite-based evaporation estimates in the Miombo differ?

*Henry M. Zimba[1,2], Miriam Coenders-Gerrits[1], Kawawa E. Banda[3], Petra Hulsman[4], Nick van de Giesen[1], Imasiku A. Nyambe[3], Hubert. H. G. Savenije[1].

[1] Water Resources Section, Faculty of Civil Engineering and Geosciences, Delft University of Technology, Stevinweg 1, 2628 CN Delft, The Netherlands.

[2] Department of Agriculture, Ministry of Agriculture, P.O. Box 50595, Mulungushi House, Independence Avenue, Lusaka, Zambia.

[3] Integrated Water Resources Management Centre, Department of Geology, School of Mines, University of Zambia, Great East Road Campus, Lusaka, Zambia.

[4] Ghent University, Hydro-Climate Extremes Lab (H-CEL), Coupure links 653, 9000 Ghent, Belgium

*Corresponding author: a.m.j.coenders@tudelft.nl

Abstract

The miombo woodland is the largest dry woodland formation in sub-Saharan Africa, covering an estimated area of 2.7 – 3.6 million km^2. Compared to other global ecosystems, the miombo woodland demonstrates unique interactions between plant phenology and climate. For instance, it experiences an increase in leaf area index (LAI) during the dry season. However, due to limited surface exchange observations in the miombo region, there is a lack of information regarding the effect of these properties on miombo woodland evaporation. It is crucial to have a better understanding of miombo evaporation for accurate hydrological and climate modelling in this region. Currently, the only available regional evaporation estimates are based on satellite data. However, the accuracy of these estimates is questionable due to the scarcity of field estimates with which to compare. Therefore, this study aims to compare the temporal dynamics and magnitudes of six satellite-based evaporation estimates (FLEX-Topo, GLEAM, MOD16, SSEBop, TerraClimate, and WaPOR) during different phenophases in the miombo woodland of the Luangwa Basin, a representative river basin in southern Africa. The goal of this comparison is to determine if the temporal dynamics and magnitudes of the satellite-based evaporation estimates align with the documented feedback between miombo woodland and climate. In the absence of basin-scale field observations, actual evaporation estimates based on the multi-annual water balance (E_{wb}) are used for comparison. The results show significant discrepancies among the satellite-based evaporation estimates during the Dormant and Green-up/Mid-Greenup phenophases. These phenophases involve substantial changes in miombo species' canopy phenology, including the co-occuring of leaf-fall and leaf-flush, as well as access to deeper moisture stocks to support leaf-flush in preparation for the rainy season. During the Green-up/Mid-Greenup phenophase, the satellite-based evaporation estimates differ significantly, while the best agreement is observed during the senescence phenophase, which corresponds to the period with high temperature, high soil moisture, high leaf chlorophyll content, and the highest LAI (i.e., the rainy season). In comparison to basin-scale actual evaporation, all six satellite-based evaporation estimates appear to underestimate evaporation. Satellite-based evaporation estimates do not accurately represent evaporation in this data-sparse region, which has a phenology and seasonality that significantly differ from the typical case in data-rich ground-truthing locations. This may also

45   be true for other locations with limited data coverage. Based on this study, it is crucial to conduct field-based observations of evaporation during different miombo species phenophases to improve satellite-based evaporation estimates in miombo woodlands.

1   Introduction

Vegetation phenology refers to the periodic biological life cycle events of plants, such as
50   leaf-flushing, senescence and corresponding temporal changes in vegetation canopy cover (Stckli et al., 2011;Cleland et al., 2007). Plant phenology and climate are highly correlated (Pereira et al., 2022; Schwartz, 2013; Cleland et al., 2007). Plants respond to triggers, such as temperature, hydrology and day light, by initiating among others: leaf-fall, leaf-flush, budburst, flowering and variation in photosynthetic activity (Pereira et al., 2022; Schwartz, 2013; Cleland et al., 2007).
55   Phenological responses are species-dependent and are controlled by adapted physiological properties (Lu et al., 2006). Plant phenology controls the access to critical soil resources such as nutrients and water (Nord and Lynch, 2009). Moreover, phenological response influences plant canopy cover and affects interactions between phenology and climate. Spatial and temporal variations in canopy leaf display, i.e., due to leaf-fall and leaf-flush, influences how much radiation
60   is intercepted by plants (Shahidan et al., 2007). Intercepted radiation has shown to influence plant transpiration (Auzmendi et al., 2011; Pieruschka et al., 2010). In water limited conditions, at both individual species and woodland scales, leaf-fall reduces canopy radiation interception while leaf-flush and the consequent increase in canopy cover increases canopy radiation interception leading to increased transpiration (Snyder & Spano, 2013), controlled by moisture availability, whether in
65   the vegetation itself or in the root zone (Tian et al., 2018). Plant canopy cover and its interactions with atmospheric carbon dioxide influences transpiration (Marchesini et al., 2015). Ultimately, plant phenological response to changes in the triggers influences transpiration and actual evaporation of the woodland (i.e. Marchesini et al, 2015).

Miralles et al. (2020) defined evaporation as "the phenomenon by which a substance is
70   converted from its liquid into its vapour phase, independently of where it lies in nature". In this study we adopt the term evaporation for all forms of terrestrial evaporation, including transpiration by leaves, evaporation from intercepted rainfall by vegetation and woodland floor, soil evaporation, and evaporation from stagnant open water and pools (Savenije, 2004). Evaporation of woodland surfaces accounts for a significant portion of the water cycle over the terrestrial
75   landmass (Sheil, 2018; Van Der Ent et al., 2014; Gerrits, 2010; Van Der Ent et al., 2010). Understanding the characteristics of evaporation, such as interception and transpiration, in various woodland ecosystems is key to monitoring the climate impact on woodland ecosystems and for hydrological modelling and the management of water resources at various scales (Kleine et al., 2021); Bonnesoeur et al., 2019); Roberts, 2013). Knowledge of the woodland phenology
80   interactions with climate variables and seasonal environmental regimes is key to this understanding (Zhao et al., 2013).

Environmental variables such as precipitation and temperature influences plant phenology differently across the diverse ecosystems globally (Kramer et al., 2000;Forrest et al., 2010;Forrest and Miller-Rushing, 2010). Additionally, Tian et al. (2018) showed that, at the ecosystem scale,
85   plants have adapted to local climatic (such as precipitation, temperature, and radiation) and abiotic (such as soil type and soil water supply) conditions. The findings by Tian et al. (2018) are "evidence of global differences in the interaction between plant water storage and leaf phenology". Although this study referred to within-plant storage of moisture it may be as relevant to root zone storage or access to groundwater. Therefore, understanding the interactions between plant

90   phenology and climate at local and regional scales and appropriately incorporating these aspects in hydrological and climate modelling is likely to improve accuracy of the simulations (Forster et al., 2022).

        The miombo woodlands is the largest dry woodland formation in sub-Sahara Africa with a spatial extent approximated between $2.7 - 3.6$ million km^2, covering about 10% of the continent
95   (Ryan et al., 2016; Guan et al., 2014; White, 1983). Despite their significance for biodiversity (Mittermeier et al., 2003, White, 1983), carbon sink (Pelletier et al., 2018) and the food, energy and water nexus (Beilfuss, 2012; Campbell et al., 1996; Frost, 1996), little attention has been paid to its hydrological functioning. The uniqueness of the interactions between plant phenology and climate in the miombo woodland has been highlighted (Tian et al. 2018; White 1983) and has been
100   particularly demonstrated by Tian et al. (2018), Vinya et al. (2018), Fuller (1999), (Frost 1996) and White (1983). Of particular importance is its control of leaf phenology (i.e., Vinya et al., 2018), co-occurring of leaf-fall (leaf shedding) and leaf-flush (i.e., Fuller, 1999), and deep rooting, which allows miombo species to access deep soil moisture, including groundwater, to buffer for dry season water limitations (Tian et al. 2018; Guan et al., 2014; Savory, 1963). Most remarkably, new
105   leaf-flushing occurs before the commencement of seasonal rainfall (Chidumayo, 1994; Fuller and Prince, 1996). Young flushed leaves in the dry season have high water content of up to 66% which declines to about 51% as the leaves harden, until they are shed off in the next season (Ernst and Walker, 1973). The miombo woodland is heterogeneous with diverse plant species whose phenological response to stimuli is species-dependent (Frost 1996). For instance, leaf-fall, leaf-
110   flush and leaf colour change are triggered at different times for each species. This means that the miombo woodland is unlike other woodlands where leaf-fall and leaf-flush occur in different seasons. In the Miombo, co-occurring of leaf-fall and leaf-flush results in a woodland canopy that is variable in terms of canopy closure and greenness especially during the dry season. As a result, it has varied canopy closure ranging from 2 to about 70 percent depending on the miombo
115   woodland strata and local environmental conditions such as rainfall, soil type, soil moisture, species composition and temperature (Frost 1996). The wet miombo woodland receives mean annual rainfall above 1100 mm while the dry miombo woodland receives mean annual rainfall of less than 1100 mm (Fuller and Prince, 1996; Chidumayo, 1987; White 1983). The depth to ground water ranges between $0 - 25$ mbgl for both wet miombo woodland and dry miombo woodland,
120   although in a few places the range is between $25 - 50$ mbgl (Bonsor & Macdonald, 2011). For the wet miombo woodland with a canopy closure of about 70 percent, at any given time, there is a relatively large woodland canopy surface for radiation interception. The deep rooting in most miombo species (Savory, 1963) potentially provides access to deep soil moisture resources like observed in ecosystems globally (Fan et al., 2017; Kleidon and Heimann, 1998). It appears that in
125   the miombo woodland soil moisture increases with depth (Chidumayo, 1994; Jeffers and Boaler, 1966; Savory, 1963). As a result, the canopy provides an evaporative surface that, in combination with other environmental variables, possibly facilitates continued transpiration even during the driest periods (i.e., Li et al., 2021). Most miombo species are broad leaved with capacity for radiation interception (Fuller, 1999) and rainfall interception of up to 20% in wet miombo
130   woodland (Alexandre, 1997). These typical phenological and physiological attributes are of particular importance for evaporative processes (Forster et al., 2022; Snyder & Spano, 2013; Schwartz, 2013).

        Regardless of the uniqueness and importance of the miombo woodland, there exists scant, if any, information on its evaporation dynamics. Most of studies in the miombo woodland
135   concentrated on the characterisation of woodland plant species (e.g.: Chidumayo and Gumbo,

2010; Chidumayo 2001; Fuller, 1999; Frost 1996), its role as a carbon sink (Pelletier et al., 2018) and the social-economic relevance of the ecosystem (Frost 1996). There is ample information on the phenology of plant species (e.g.: Chidumayo and Gumbo, 2010;Chidumayo 2001); Fuller, 1999; Frost 1996), but there have been very limited attempts to characterise evaporation of the miombo ecosystem, especially during the dry season. Based on literature in public domain Zimba et al. (2023) is the only point-based field observations of evaporation of the miombo woodland. They found that all the satellite-based estimates they compared to field observations underestimated dry season and early rainy season actual evaporation in the wet miombo woodland. Furthermore, they showed that in the dry season (June-October), except for the WaPOR, the temporal dynamics of the satellite-based estimates differed from that of the field observations. These point-based estimates by Zimba et al. (2023) are not sufficient to make any definitive conclusions about the evaporative dynamics of this vast ecosystem. The study was limited in both time and space: it did not cover all the phenophases of the miombo woodland, it was only conducted in the wet miombo woodland and was limited to the point location in Mpika, Zambia. For a more expanded understanding of the evaporation dynamics of the miombo woodland there is need for comparison of satellite-based across all the phenophases: covering both the dry season and wet season in both dry miombo woodland and wet miombo woodland.

In the absence of spatially distributed field observations, satellite-based evaporation estimates are valuable alternatives, though they come with their own limitations (Zhang et al., 2016). It is well-realised that evaporation depends on land cover (Han et al., 2019; Liu and Hu, 2019; Wang et al., 2012), but, because of the differences in algorithms, process and inputs, satellite-based evaporation estimates differ for the same land surface (Cheng et al., 2021; Zhang et al., 2016). Currently, satellite-based evaporation estimates at various scales are available (e.g.: Global land evaporation Amsterdam model (GLEAM) (Martens et al., 2017; Miralles et al., 2011; Moderate-resolution imaging spectrometer (MODIS) MOD16) (Running, Steven W, Qiaozhen Mu, Maosheng Zhao, 2019; Mu et al., 2011; Mu et al., 2007); Operational simplified surface energy balance (SSEBop) (Senay et al., 2013); and Water productivity through open access of remotely sensed derived data (WaPOR) (FAO, 2018)). Classification of the various satellite-based evaporation estimates have been extensively discussed by Zhang et al. (2016), (Jiménez et al., 2011) and (Jiménez et al., 2009). Most of these satellite-based evaporation estimates were primarily developed for agricultural crops (i.e., (Biggs et al., 2015). Additionally, satellite-based evaporation estimates perform differently depending on the land surface (Cheng et al., 2021; Zhang et al., 2016). However, natural woodlands have different interactions between plant phenology and climate and evaporation characteristics (Wang-Erlandsson et al., 2016; Snyder & Spano, 2013; Schwartz, 2013). There is currently no publication in the public domain showing how various satellite-based evaporation estimates compare in the miombo woodland, especially with a focus on the unique interactions between phenology and hydrology in miombo species across different phenophases and seasons. Yet, the use of satellite-based evaporation estimates in hydrological modelling, climate modelling and the management of water resources, globally and in Africa, is increasing (i.e., García et al., 2016; Zhang et al., 2016; Makapela, 2015). However, because of the absence or scarce field observations and extremely limited validation, it is impossible to know which satellite-based evaporation estimates are close to the actual conditions of the miombo woodland. If any, the choice for a satellite-based evaporation product is based on validation results in non-miombo woodlands or at a scale (i.e., Weerasinghe et al., 2020) that includes other woodland types. For instance, an evaporation estimation approach that performs well in energy limited conditions or homogeneous woodlands (i.e., (Bogawski and Bednorz, 2014)

cannot be assumed to have the same performance in a warm, water limiting and heterogeneous woodland such as the miombo. Therefore, there is a need to validate evaporation products at the local and regional levels in order to improve the outcomes in the use of satellite-based evaporation products. Although, Weerasinghe et al. (2020) compared satellite-based evaporation estimates in the Zambezi Basin, whose vegetation cover, among many others, comprises the miombo woodland, the focus of their study was not on the miombo woodland. Furthermore, Weerasinghe et al. (2020) did not attempt to link the differences in the satellite-based evaporation estimates to the phenology of the miombo woodland. The results they observed at the Zambezi Basin scale might be different at sub-basin level such as the Luangwa Basin.

This study addresses the performance of satellite-based evaporation estimates during different phenophases of the miombo woodland with a focus on the Luangwa sub-basin of the Zambezi, one of the largest river basins in the miombo ecosystem. The Luangwa basin contains both dry (i.e., southern miombo woodlands) and wet (i.e., central Zambezian miombo woodlands) miombo. The central Zambezian miombo woodland is the largest of the four miombo woodland sub-groups, the other three being the Angolan miombo woodland, eastern miombo woodland, and the southern miombo woodland (Frost, 1996;White, 1983). The Luangwa Basin is largely covered by miombo woodland with the mopane woodland occupying a much smaller area of the basin (Frost, 1996;White, 1983). These attributes suggest a catchment that provides a fair representation of miombo woodlands and an appropriate site for studying its evaporation characteristics.

Hence, the aim of this study is two-fold:
(i)   Compare the temporal dynamics and magnitudes of six freely available satellite-based evaporation products across different phenophases of the miombo woodland.
(ii)   Compare satellite-based evaporation estimates to the water balance-based actual evaporation estimates for the Luangwa Basin.

2   Materials and Methods
2.1   Study site
The location and extent of the miombo woodland in Africa is presented in Fig. 1(a) (Ryan et al., 2016; White, 1983). The Luangwa (Fig. 1) is a sub-basin of the Zambezi Basin in sub-Saharan Africa in Zambia with spatial extent of about 159,000 km^2 (Beilfuss, 2012);(World Bank, 2010). Based on the miombo woodland delineation by White, (1983) and Ryan et al. (2016) as given in Fig.1 (b) about 75 percent of the total Luangwa Basin land-mass is covered by the miombo woodland, both dry and wet miombo. Additionally, statistics from the 2019 Copernicus land cover classification (Fig. A1 in the supplementary data), indicates that 77 % of the total basin area is woodland (dense and open woodland) which is largely miombo woodland with a smaller component of mopane woodland in the middle area of the basin (Buchhorn et al., 2020; Martins et al., 2020). Elevation (Fig. 1c) ranges between 329 – 2210 m with the central part generally a valley. The miombo woodland, both dry and wet miombo, is generally in the upland (Fig.1c). The Luangwa River, 770 km long, drains the basin and is scarcely gauged (Beilfuss, 2012). This has resulted in a paucity of data on various hydrological aspects such as rainfall and discharge. The climate is characterised by a well-delineated wet season, from October to April, and a dry season, from May to October. Furthermore, the dry season is split into the cool-dry (May to August) and hot dry (August to October) seasons. The movement of the inter-tropical convergence zone (ITCZ) over Zambia between October and April dominates the rainfall activity in the basin. The basin has a mean annual precipitation of about 970 mm yr^{-1}, potential evaporation of about 1560 mm yr^{-1}, and river runoff reaches about 100 mm yr^{-1} (Beilfuss, 2012;World Bank, 2010). The key character

of the miombo woodland species is that it sheds off old leaves and acquires new ones during the period May to October during the dry season. Depending on the amount of rainfall received in the preceding rain season the leaf-fall and leaf-flush processes may start early (i.e., in case of low rainfall received) or late (in case of high rainfall received) and may continue up to November (i.e., in the case of high rainfall received) (Frost,1996).
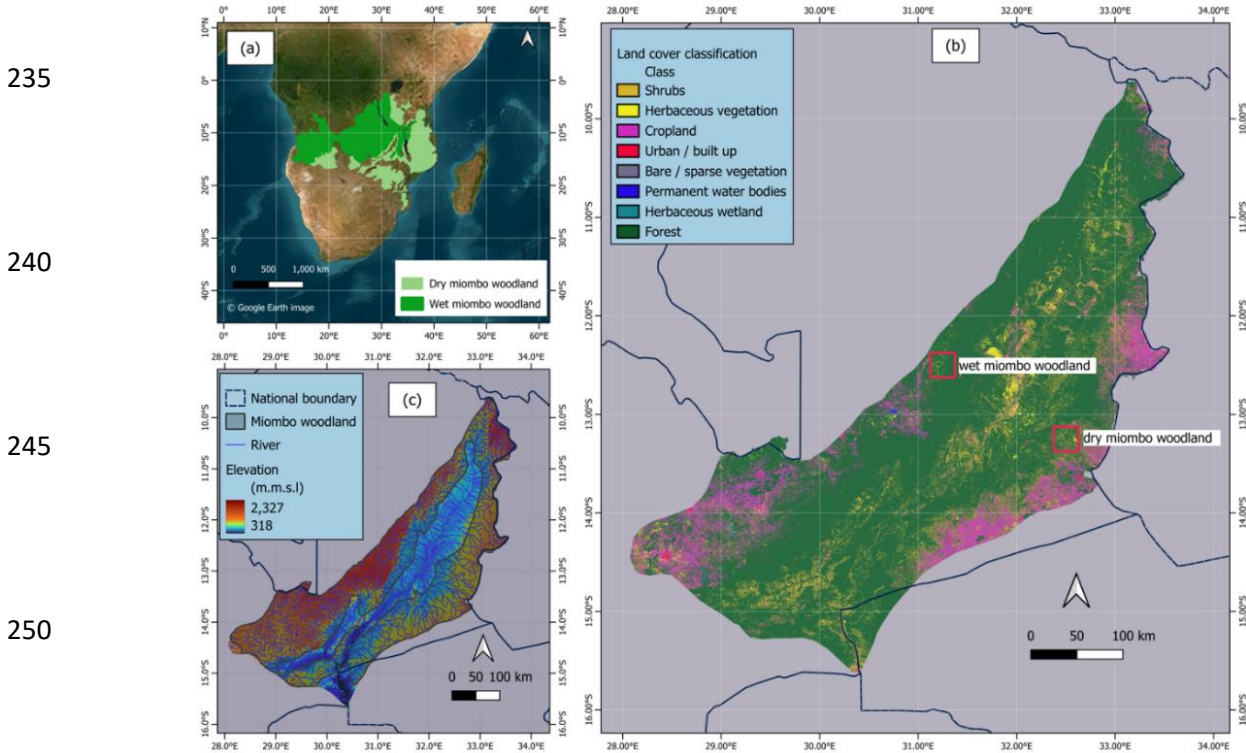
Figure 1: (a) Spatial extent of the miombo woodland in Africa and the location of the Luangwa Basin in Zambia. (b) Land cover characterisation of the Luangwa Basin based on the Copernicus land cover classification. (c) Spatial distribution of elevation ASTER digital elevation model (DEM) and the extent of the miombo woodland in the Luangwa Basin.

2.2 Study approach

The study sought to find out the extent to which satellite-based evaporation estimates agree with each other during the different canopy phenophases of the miombo woodland. Point scale observations in the wet miombo woodland (Zimba et al., 2023) showed that satellite-based evaporation estimates underestimated actual evaporation of the wet miombo woodland during the dry season and early rainy season in the Luangwa Basin. However, the Luangwa Basin has a heterogenous land cover which includes mopane woodland and grasslands. The question was whether the heterogeneity in the land cover of the Luangwa Basin would result in satellite-based evaporation estimates performing contrary to the point-scale observations at a wet miombo woodland site when compared to the water balance-based evaporation estimates at basin scale.

For this study, a 12-year period, 2009–2020, was used because satellite-based evaporation estimates were available for free for this period. The period also had cycles of low and high annual rainfall allowing to analyse performance under changing monthly and annual conditions. The following sections elaborate the methods used in this study.

2.2.1 Phenophases of the miombo woodland and assessment of phenological conditions

To categorise the phenophases two approaches were used: climate and soil moisture-based classifications and satellite-based classifications.

For the climate and soil moisture-based classification (Chidumayo and Frost, 1996) observed five phenological seasons: warm pre-rainy season, early rainy season, mid-rainy season, late rainy season and the cool dry season (Fig. 2). For easy of analysis, the above three rainy season phenophases were merged into one rainy season phenophase. Therefore, three climate and soil moisture-based phenophases were established; warm pre-rainy season, rainy season and the cool dry season. Satellite-based classification of phenophases has been based on the National Aeronautics and Space Administration (NASA) Collection 6 MODIS Land Cover Dynamics (MCD12Q2) Product accessed from the https://modis.ornl.gov/globalsubset/, last access: 20 February, 2023 (Gray et al., 2019; Zhang et al., 2003). The MCD12Q2 uses the changes in canopy greenness to characterise the canopy phenophases (Gray et al., 2019). For the miombo woodland in the Luangwa Basin eight phenophases were identified using the satellite-based data MCD12Q2 (Fig. 2). The satellite-based phenophases include: green-up, mid-green up, maturity, peak, senescence, green-down, and mid-green down and dormant. For easy of analysis the phenophases were merged into four groups based on dominant activity in each phenophase (Fig. 2). To compliment the MCD12Q2 classification the MODIS-based leaf area index (LAI) obtained from https://modis.ornl.gov/globalsubset/, last access: 20 February, 2023) (Myneni et al., 2021; ORNL DAAC, 2018; Myneni & Park, 2015) and the normalised difference vegetation index (NDVI) (ORNL DAAC, 2018; Vermote and Wolfe, 2015) were used.
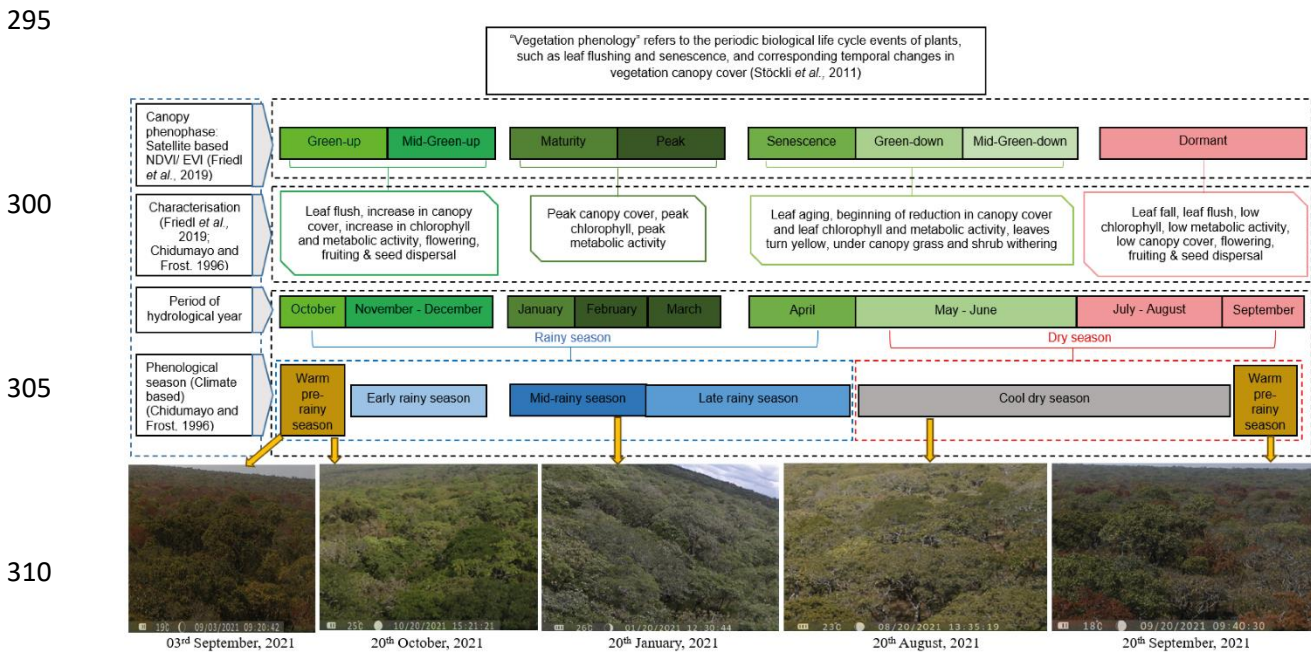
Figure 2: Characterisation of canopy phenophases of the miombo woodland in relation to seasonality for the Luangwa Basin. Photographs show the changes in the canopy cover on selected days across different phenophases of a wet miombo woodland at the Mpika site (Lat: 12.387454°S; Long: 31.170911°E) for the year 2021.

The satellite-based LAI and NDVI have been used before as proxies to observe phenological conditions such as the canopy biomass formation, changes in the canopy closure (i.e.,

320 through leaf-fall and leaf-flush) and changes in canopy chlorophyll conditions (Guan et al., 2014; Santin-Janin et al., 2009; Chidumayo, 2001; Fuller, 1999). For the LAI the NASA's MCD15A3H product (Myneni, Knyazikhin & Park, 2021; ORNL DAAC, 2018; Myneni & Park, 2015) with a four-day temporal resolution and 500 m spatial resolution has been used. The MODIS MOD09GQ.006 (Vermote and Wolfe, 2015) surface reflectance bands 1,5 and 6 have been used
325 to estimate the NDVI at daily temporal resolution and 250 m spatial resolution using the band ratio method. The daily NDVI values were then averaged into four-day values to obtain the same temporal resolution as the LAI.

To mitigate potential confusion arising from the use of dual phenophase classifications, this study exclusively employs satellite-based phenophases for analysis purposes. Within these
330 phenological seasons the phenology of miombo species transitions through various stages i.e., from leaf-fall/leaf-flush, growth of stems, flowering to mortality of seed (Chidumayo and Frost,1996).

To compliment the observations, photographs from a digital camera (Denver WCT-8010) installed on the flux tower at a wet miombo woodland site in Mpika (Zimba et al., 2023) were used
335 to observe the changes in the canopy phenology of the miombo woodland across different phenophases from January to December in the year 2021. In addition, the fish-eye (LIEQI LQ-001) was used to obtain canopy images. The images of the canopy helped to observe the changes and differences in canopy leaf display (i.e., leaf-fall, leaf-flush and leaf colour changes) among miombo species.
340

2.2.2 Delineation of the miombo woodland areas used in this study

The satellite-based evaporation estimates were compared to each other using grids at two known sites representing the dry miombo woodland and wet miombo woodland and at the entire miombo woodland scale in the Luangwa Basin (Figs. 1 and 3).

345
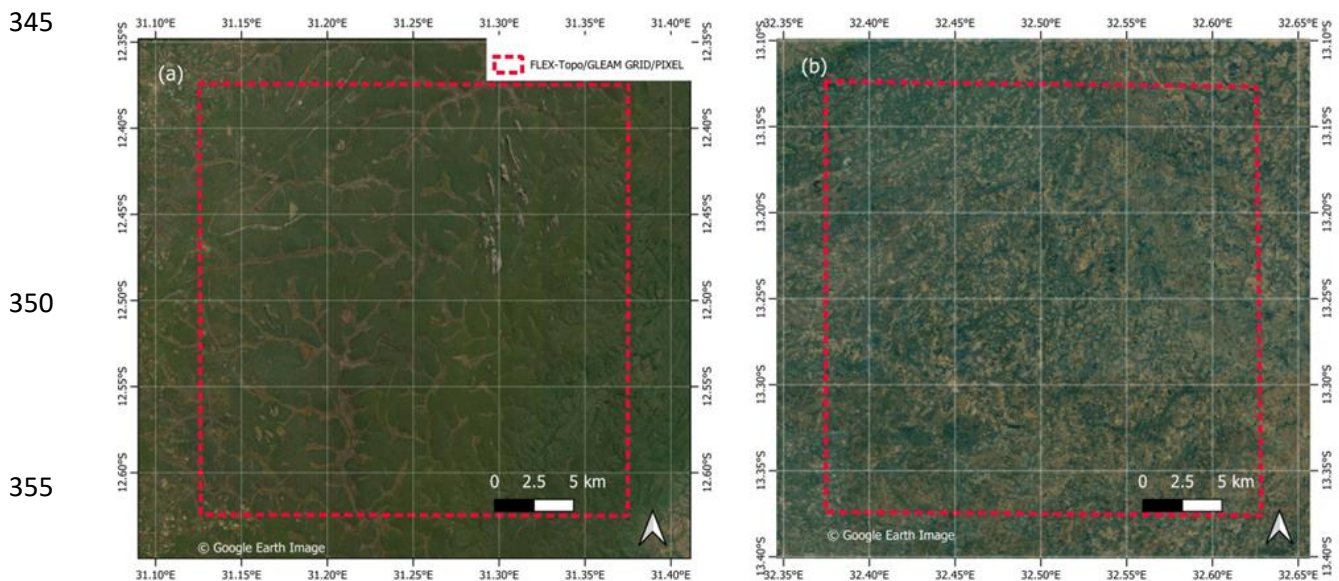
Figure 3: The wet miombo woodland (a) and dry miombo woodland (b) locations used for
360 comparison of satellite-based evaporation estimates at FLEX-Topo and GLEAM spatial resolution (approximately 27.7 km by 27.7 km). The dotted red line is the actual location of the FLEX-Topo and GLEAM pixels.

Firstly, a comparison based on the 27.7km by 27.7km grid was performed by using known undisturbed dry miombo woodland and wet miombo woodland locations (Figs. 1 and 3). The grid was based on the satellite-based evaporation estimates (i.e., FLEX-Topo and GLEAM) with the largest spatial resolutions (approximately 27.7 km by 27.7 km) (Fig. 3 and Table 1). For MOD16, SSEBop, TerraClimate and WaPOR, the mean of aggregated actual evaporation estimates in all the pixels within the dotted red square (Fig. 3) were used. In the same way the mean of the aggregated NDVI and LAI values in all the pixels within the dotted red square were used for analysis. The focus on a known wet miombo woodland enabled comparison of the field observations of the changes in canopy cover using digital camera images to the satellite-based LAI and NDVI for the year 2021. See Section 2.2.3 and Table 1 for satellite-based evaporation estimates used in this study. Secondly, the typical miombo woodland regions as categorised by (White, 1983) and (Ryan et al., 2016) (see Fig. 1 a, b) were used to delineate the area covered by the miombo woodland in the Luangwa Basin. The delineated miombo woodland in the Luangwa Basin excluded the mopane woodland, mixed woodland as well as the water bodies. This delineation (as shown in Fig. 1) ensured that only the areas classified as typical miombo woodland (Ryan et al., 2016; White, 1983) were considered in the analysis.

2.2.3 Satellite-based products used in the study

The six satellite-based evaporation estimates consisted of: 1) FLEX-Topo (Hulsman et al., 2021;Hulsman et al., 2020; Savenije, 2010); 2) Thornthwaite-Mather climatic water balance model (TerraClimate) (Abatzoglou et al., 2018); 3) Global land evaporation Amsterdam model (GLEAM) (Martens et al., 2017; Miralles et al., 2011); 4) Moderate-resolution imaging spectrometer (MODIS) MOD16 (Running, Steven W, Qiaozhen Mu, Maosheng Zhao, 2019; Mu et al., 2011; Mu et al., 2007); 5) Operational simplified surface energy balance (SSEBop) (Senay et al., 2013b) and 6) Water productivity through open access of remotely sensed derived data (WaPOR) (FAO, 2018). These satellite-based evaporation estimates were selected purely because they are free of charge and easily accessible from various platforms and have an archive of historical data with the temporal and spatial resolutions suitable for use in this study. Except for FLEX-Topo and GLEAM (with spatial resolution of 27.7 km), these satellite-based evaporation estimates have relatively fine spatial resolution (i.e., 500 m, 1000 m, 4000 m and 250 m for MOD16, SSEBop, TerraClimate and WaPOR respectively) and temporal resolution (daily, 8-day, 10-day and monthly respectively), which attributes were suitable for this study. The original spatial resolutions were used because these satellite-based evaporation estimates are normally used as is, in their original resolutions. Resampling the different spatial resolutions of the satellite-based evaporation estimates to a single (uniform) spatial resolution was thought to be problematic as it would have introduced unknown and unquantifiable errors, regardless the extent resampled. For detailed explanations on the model structure, processes and inputs for the satellite-based evaporation estimates used in this study the reader is advised to refer to the cited literature above and in Table 1.

Other satellite-based products used in this study include the ASTER digital elevation model (DEM) (Abrams and Crippen, 2019), MODIS-based LAI and NDVI, Copernicus land cover map, net radiation, precipitation, runoff, soil moisture and relative humidity. For detailed information (i.e., structure, processes and inputs) on the other satellite-based products used in this study the reader is advised to refer to the cited literature in Table 1.

Table 1. Characteristics of products used in the study

Variable	Product name	Time Period	Spatial coverage/Location	Temporal resolution	Spatial resolution	Reference	Source of data
Precipitation	CFSR v2	2009 - 2020	Global	Daily	19.2 km	(Saha et al., 2014; Saha et al., 2010)	Climate Engine portal
	CHIRPS	2009 - 2020	Global	Daily	4.8 km	(Funk et al., 2015)	https://app.climateengine.com/climateEngine
	ERA5	2009 - 2020	Global	Daily	24	(Hersbach et al., 2017)	Climate Engine portal
Air temperature (mean)	TerraClimate	2009 - 2020	Global	Monthly	4 km	(Abatzoglou et al., 2018)	Climate Engine portal
	CFSR v2	2009 - 2020	Global	Daily	19.2 km	(Saha et al., 2014; Saha et al., 2010)	Climate Engine portal
LAI	MODIS MCD15A3H v6	2021	Global	4-Day	0.5 km	(Myneni, Knyazikhin & Park, 2015)	Climate Engine portal
NDVI	MODIS MOD09GA v6	2021	Global	Daily	0.5 km	(Vermote & Wolfe, 2015)	Climate Engine portal
Runoff	Observations	1960-1992	159,000 km²	Daily	N/A		WARMA, Zambia
	TerraClimate	1960 - 2020	Global	Monthly	4 km	(Abatzoglou et al., 2018)	Climate Engine portal
Net radiation	CFSR v2	2009-2020	Global	Daily	19.2 km	(Saha et al., 2014; Saha et al., 2010)	Climate Engine portal
Soil moisture (25 cm)	CFSR v2	2009-2020	Global	Daily	19.2 km	(Saha et al., 2014; Saha et al., 2010)	Climate Engine portal
Relative humidity	CFSR v2	2009 - 2020	Global	Daily	19.2 km	(Saha et al., 2014; Saha et al., 2010)	Climate Engine portal
Elevation	ASTER GDEM v3	N/A	Global	N/A	30m	(Abrams and Crippen, 2019)	NASA Glovis portal
Land cover map	Copernicus CGLS-LC100 v3	2019	Global	Annual	100m	(Buchhorn et al., 2020)	Google Earth Engine
Actual evaporation	FLEX-Topo	2009 - 2020	Catchment	Daily	27.7 km	(Hulsman et al., 2021; Hulsman et al., 2020; Savenije, 2010)	ZAMSECUR Project – Delft Technical University
	GLEAM (v3.2a)	2009 -2020	Global	Daily	27.7 km	(Martens et al., 2017; Miralles et al., 2011)	GLEAM FTP server
	MOD16v2	2009 -2020	Global	8-Day	0.5 km	(Running et al., 2019; Mu et al., 2011)	Climate Engine portal; Global subsets tool: MODIS/VIIRS Land Products
	SSEBop	2009 -2020	Global	Monthly	1 km	(Senay et al., 2013).	Climate engine portal
	TerraClimate	2009 -2020	Global	Monthly	4 km	(Abatzoglou et al., 2018)	Climate engine portal
	WaPOR v2 (ETLook)	2009 -2020	Continental	10-Day	0.25 km	(FAO, 2018)	WaPOR Portal

2.2.4 Actual evaporation derived from the water balance

In cases where spatially distributed field measurements are not available the water balance approach, using spatially distributed satellite-data, is a practical approach (i.e., Weerasinghe et al., 2020; Liu et al., 2016). In this study the general annual water balance was used to test the performance of the satellite-based evaporation estimates at basin level.

The basin average annual water balance-based evaporation ($E_{a_{(wb)}}$) is estimated using Eq. (1) where long-term over-year storage change is disregarded.

$$E_{a_{(wb)}} = P - Q \qquad\qquad [1]$$

where, P is the annual average catchment precipitation in mm year^{-1} and Q is annual average discharge in mm year^{-1}. The precipitation and discharge information for the water balance approach were selected and used as explained below.

Ensemble satellite precipitation

The challenge posed by using satellite-based precipitation data in African catchments is that most, if not all, satellite precipitation products are geographically biased towards either underestimation or overestimation, despite some of them having good correlation with ground observations (Macharia et al., 2022;Asadullah, McIntyre, & Kigobe, 2008). The lack of adequate ground precipitation observations makes it difficult to validate, as well as correct, the product's bias with an acceptable degree of certainty. There is not a single precipitation product that has been found to perform better than other precipitation products across African landscapes and southern Africa in particular (Macharia et al., 2022). For the Luangwa Basin there is no guarantee that any of the precipitation products are spatially representative of a basin that is about 159,000 km^2 with varying topographical attributes. For instance, compared to point-based field observations of precipitation at six weather stations in Zambia (three stations in the Luangwa Basin and the other three outside of the Luangwa Basin) no single satellite-based precipitation product showed consistency with all weather stations (see Table A1 in the supplementary data). Using an ensemble of precipitation products is said to reduce errors and is therefore recommended (e.g.: Weerasinghe et al., 2020; Asadullah et al., 2008). When the annual mean of an ensemble of four satellite-based precipitation products was compared to annual means of field observations at different weather stations the margin of either underestimation or overestimation was reduced (See Table A1 in supplementary data). To this extent, for the general water balance, this study used annual mean of four satellite precipitation products. The four precipitation products are the Climate Forecasting System Reanalysis (CFSR), Climate Hazards Group Infra-Red Precipitation with Station data (CHIRPS), ECMWF Reanalysis v5 (ERA5) and TerraClimate (see Table 1). These satellite precipitation products were selected purely based on availability and the fact that they are spatially distributed and cover the entire Luangwa Basin (Table 1). Field observations of precipitation for GART Chisamba (data for the period 2020 – 2022) and Lusaka International Airport, Kabwe, Mwinilunga and Serenje weather stations for the years 2014 - 2016 were obtained from the Southern African Science Service Centre for Change and Adaptive Land Management (SASSCAL) weathernet (Last accessed: 20 January, 2023: http://www.sasscalweathernet.org). The observations for Mpika for the year 2021 were obtained from the ZAMSECUR project dataset available at 4TU.ResearchData repository (https://doi.org/10.4121/19372352.v2) (Zimba et al., 2022). Three weather stations, GART Chisamba, Lusaka International Airport and Mwinilunga, are outside of the Luangwa Basin and were used for comparison purposes only. However, GART

500 and Lusaka International airport stations are very close to the Luangwa Basin. The other three stations Kabwe, Serenje and Mpika are within the Luangwa Basin (see Table A1 in the supplementary data for location coordinates of the weather stations). Nevertheless, the results of the comparison of satellite precipitation products with field observations were similar (underestimation or overestimation) at all weather stations both in the Luangwa Basin and outside
505 the basin (See Table A1 in the supplementary data).

Estimating runoff data

Reliable monthly basin-scale field observations of runoff were only available for the period 1961 -1992 and not for the study period 2009 – 2020. Monthly modelled TerraClimate runoff data
510 (Abatzoglou et al., 2018) was available for the period 1958 – 2020. The shapefile for the entire Luangwa Basin was used as boundary for the gridded TerraClimate run-off and obtain the basin scale average run-off. The basin scale average of TerraClimate run-off was then compared with the observed Luangwa Basin run-off. Compared to field observations the average TerraClimate runoff data was significantly higher during the peak rainfall period of January-February. At annual
515 scale TerraClimate overestimated runoff data but strongly correlated (r = 0.83) with field observations (Fig. 4a).
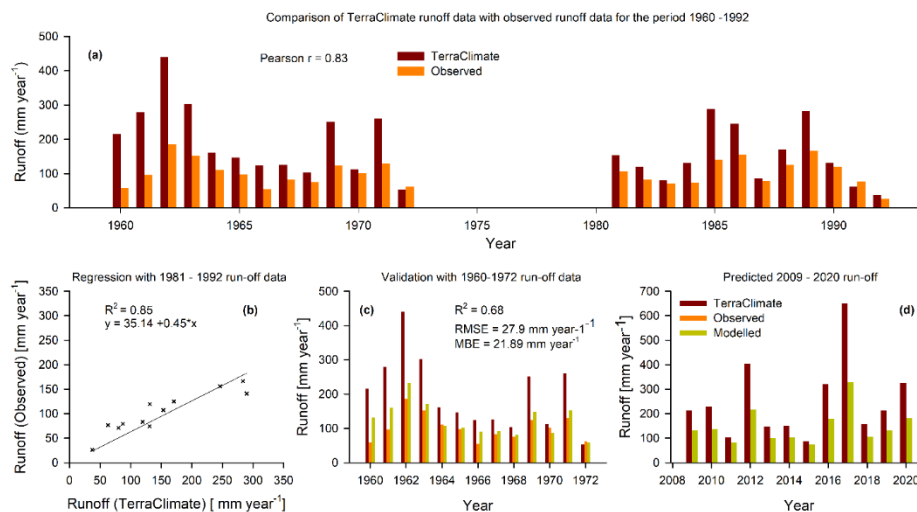
520

525

Figure 4: Procedure for extending near field observations runoff data for the period 2009-2020
530 using the TerraClimate runoff data as the predictor. (a) annual time series of observed runoff and TerraClimate runoff for the period 1960 - 1992, (b) regression of observed runoff with TerraClimate runoff for the period 1981 – 1992, (c) validation of the regression model for predicting runoff using the 1960 – 1972 observed runoff data and (d) comparison of predicted TerraClimate runoff using the regression model with original TerraClimate run-off time series.
535

Based on the correlation of annual TerraClimate runoff data with field observations a linear regression equation was formulated to help generate extended near field observations time series for the period 2009-2020. TerraClimate runoff data was used as predictor variable. The TerraClimate runoff data was used because of availability free of cost and with relatively fine
540 temporal and spatial resolution (monthly and 4 km respectively) (Table 1). Firstly, the field observations runoff data and TerraClimate runoff data for the period 1960 - 1992 were split into two segments, 1960 - 1972 and 1981 - 1992. The runoff data for the period 1981 -1992 was used

as training data to generate a linear equation with the TerraClimate runoff data as the predictor variable (Fig. 4b). The generated linear equation was validated using the 1961-1972 TerraClimate runoff data as a predictor variable (Fig. 4c). The predicted 1961-1972 runoff data with the TerraClimate runoff data as a predictor variable was then compared to the field observations for the same period (Fig. 4 c). The performance statistics of the equation showed $R^2 = 0.68$, RMSE = 27.9 mm year^{-1} and mean bias error (MBE) = 21.9 mm year^{-1} (Fig. 4 c). The linear regression equation was then used to generate near field observations runoff data for the period 2009 – 2020 with TerraClimate runoff data for the same period as the predictor variable (Fig. 4 d). Generally, both for the observed and extended time series (with TerraClimate data as predictor) the annual runoff coefficient was 11%. The near field observations extended runoff data was then used in the water balance approach, as explained in Section 2.2.4 Eq. (1), to estimate actual evaporation at basin level.

2.2.5 Time series pre-processing and statistical analyses
Deseasonalising time series
The presence of seasonal variations in hydrological time series can complicate data analysis and hinder the identification of underlying trends and patterns. Deseasonalising (removing seasonality) the data can provide a clearer understanding of its long-term behaviour and prevent false results. The centred moving average (CMA) and adjusted seasonal factor (ASF) are among the various commonly used methods to deseasonalise time series (Ghysels et al., 2006; Nelson et al., 1999; Briuinger et al., 1983). To prepare for statistical analyses, the original time series of evaporation, LAI, and NDVI were deseasonalised using the CMA and ASF approach. Firstly, the time series were examined for the presence of seasonality. Once a 12-month lag seasonal component was detected, the time series were deseasonalised. This involved calculating the CMA using Eqs. (2) and (3). The ASF was estimated by dividing the original time series by the CMA, as indicated in Eq. (4). Then, the original monthly time series were deseasonalised by dividing them by the ASF of each variable, as given in Eq. (5).

$$X^*_{t+.5} = \sum_{j=-\left(\frac{S}{2}\right)+1}^{S/2} X_{t+j} \left(t = \frac{S}{2}, \frac{S}{2} + 1, \frac{S}{2} + 2, \ldots, n - \frac{S}{2} \right) \qquad [2]$$

To estimate a centred moving average (X^*_t) eq. 3 is used.

$$X^*_t = \frac{X^*_{t-.5} + X^*_{t+.5}}{2} \left(t = \frac{S}{2}, \frac{S}{2} + 1, \frac{S}{2} + 2, \ldots, n - \frac{S}{2} \right) \qquad [3]$$

$$ASF = \frac{X_t}{X^*_t} \qquad [4]$$

$$X_{td} = \frac{X_t}{ASF} \qquad [5]$$

where X_t is the original variable estimate for each month, ($X^*_{t+.5}$) is the moving average value, X^*_t is the centred moving average value, S is the even number of the lag of the seasonal component, 12 in the case of this study and n is the total number of time series and ASF is the adjusted seasonal factor and X_{td} is the deseasonalised time series. In order to assess the degree of deviation between original time series and deseasonalised time series, with the purpose of identifying anomalous

occurrences within the data, the original monthly time series were subtracted by the deseasonalised
580   time series (Eq. 6).

$$Anomaly = X_t - X_{td} \qquad\qquad [6]$$

Therefore, for statistical analyses the original time series, deseasonalised time series and the
anomalies were utilised in this study.

Statistical analyses

585   The Mann-Kendal trends test (Helsel et al., 2020), a non-parametric statistical model, was
used to evaluate the overall temporal trend in satellite-based evaporation estimates. The coefficient
of variation (CV) (%) in Eq. (7) (Helsel et al., 2020) was used to understand the extent to which
the satellite-based evaporation estimates varied between each other for each phenophase. When
evaluating temporal variations in individual satellite-based evaporation estimates, high
590   coefficients of variation (CVs) in certain phenophases may not necessarily indicate uncertainties
in estimating evaporation. Instead, they could be a result of temporal variations in climate variables
such as leaf area, rainfall, soil moisture, and temperature. On the other hand, when comparing the
means of different satellite-based evaporation estimates over a specific phenophase, high CV
values indicate larger differences between the means of individual evaporation estimates. In this
595   case, these high CVs may be indicative of differences in the ability to estimate evaporation in that
phenophase by an individual satellite-based evaporation estimate.

$$CV = \frac{\bar{x}}{\bar{s}} \qquad\qquad [7]$$

600   where $\bar{x}$ is mean of the observations and $\bar{s}$ the standard deviation. The higher the CV value,
the larger the standard deviation compared to the mean, which implies greater variation among the
variables.
              Furthermore, the analysis of variance (ANOVA) (Helsel et al., 2020) and all pairwise
multiple comparison procedures with the Tukey Test (Helsel et al., 2020) were performed. The
605   ANOVA and the pairwise comparison assisted in observing the satellite-based evaporation
estimates that were significantly different in magnitudes in each phenophase. The study examined
the correlations between satellite-based evaporation estimates, specifically focusing on their
similarity in temporal dynamics. This assessment was conducted at both monthly and annual scales
using two different techniques: the non-parametric Kendal correlation test (Helsel et al., 2020) and
610   the parametric Pearson correlation (Helsel et al., 2020). The choice between these two techniques
depended on the results of the normality test conducted on the time series data. To establish the
extent to which the satellite-based evaporation estimates underestimated or overestimated
evaporation, relative to E_{wb}, the mean bias error (Eq. 8) is used:

615     $$MBE = \frac{1}{n}\sum_{i=1}^{n}(E_{s_i} - E_{a_{(wb)}}{}_i) \qquad\qquad [8]$$

where n is the number of annual data used, $E_{a(wb)}$ is the water balance-based actual evaporation
time series and E_s is the satellite-based evaporation estimates time series. The smaller the mean
bias error value (positive or negative), the less the deviation of the predicted values from the water
620   balance obtained values (Helsel et al., 2020).

3   Results and discussion
3.1   Basin scale miombo woodland climate and phenological temporal dynamics(s)

Figure 5 shows Luangwa Basin miombo woodland (area delineated as miombo woodland only in Fig. 1c) aggregated 2009-2020 MODIS NDVI and CFSR data climate conditions: net radiation (R_N), air temperature (T_a), relative humidity (RH), soil moisture (SM) and precipitation (P). The peak atmospheric and phenological variables values were observed in the early and mid-rainy seasons during the green-up and maturity/peak phenophases. The lowest values in atmospheric and phenological variables were observed in the cool dry season during the green-down and dormant phenophases. Net radiation, air temperature, relative humidity covaried (positively or negatively) with the NDVI (proxy for canopy phenology) depending on the phenophase (Fig. 5 and Fig. A2 in the supplementary data).
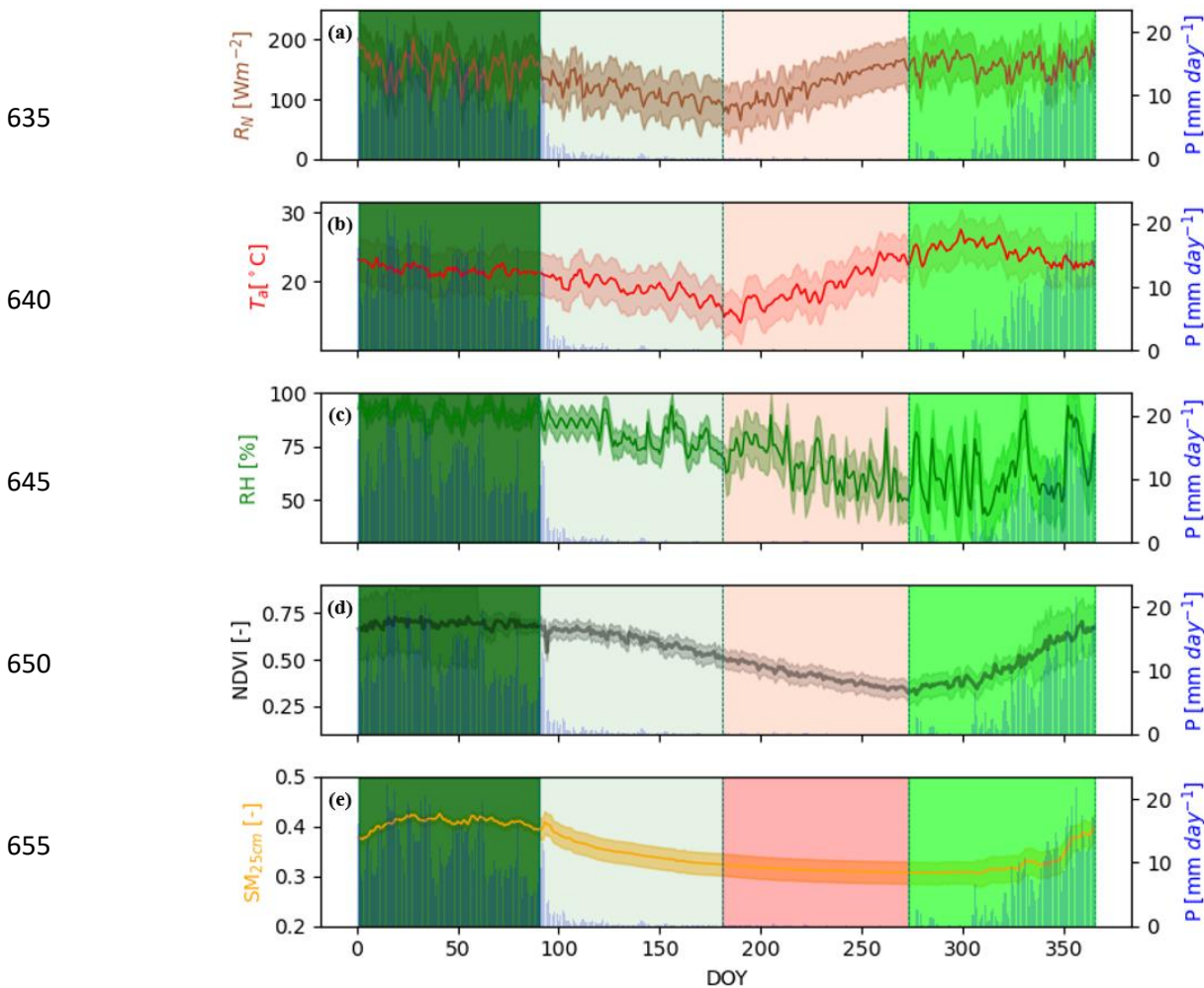
Figure 5: Luangwa Basin miombo woodland spatially and temporally aggregated 2009-2020 daily atmospheric conditions: (a) net radiation (R_N), (b) air temperature (T_a), (c) relative humidity (RH), (d) phenological conditions proxied by the NDVI, and (e) soil moisture (SM) plotted against precipitation (P). The shaded areas represent the phenophases as used in this study: January – March is the peak/maturity, April – June is the senescence/green-down, July – September is the dormant and October – December is the green-up/mid-green-up phenophase. Shaded area for variables is the standard deviation. DOY is the day of the year.

The strong correlation between climate and phenology (i.e., NDVI and air temperature/soil moisture) in the miombo woodland (Fig. A2 in the supplementary data) agreed with observations made by Chidumayo (2001) and in other ecosystems (Pereira et al., 2022; Schwartz, 2013; Cleland et al., 2007).

3.2   Observed phenological conditions in the miombo woodland

Fuller (1999) observed that the canopy closure is varied, ranging between 2 percent to about 70 percent in the shrub, dry miombo woodland and wet miombo woodland. Therefore, depending on location and dominant species, exposure of the understorey, field, and ground layers to incident solar radiation through the canopy is substantial (Fig. 6, Chidumayo, 2001; Fuller, 1999).
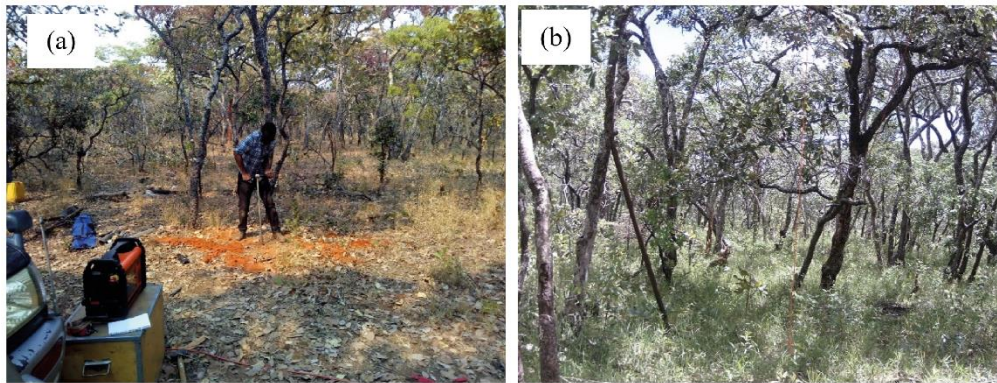
Figure 6: Dry season (a) and rainy season (b) tree layer, understorey, and field layer conditions at the wet miombo woodland site (Lat: 12.387454°S; Long: 31.170911°E) in Mpika, Zambia. Images taken on 29th September and 23rd December, 2021.

In the dry season, the grass in the field layer and some understorey non-deep rooting shrubs die back when moisture is scarce. During dry periods, they survive by entering a dormant state with buds located near the soil surface (Fig. 6a and Chidumayo, 2001, Fuller, 1999). Hence, the changes in total LAI and NDVI in the phenophases in the dry season can largely be attributed to the changes in the tree layer of the miombo species (i.e., Fig. 6a, Fig. 7 and Chidumayo, 2001). The field layer during the rainy season mainly comprises green grass (Fig. 6b and Chidumayo, 2001). Therefore, total LAI and NDVI in phenophases in the rainy season can be largely attributed to both the field layer i.e., grass, understorey, and the tree layer, i.e.: shrubs and tree canopy (i.e., Fig. 6b and Chidumayo, 2001). The LAI and NDVI were used as proxies to observe the changes in the canopy cover across different phenophases of the miombo woodland. At a 27.7km-by-27.7km grid scale (Fig. 8a) the spatial distribution and mean of the aggregated values of the LAI and NDVI for the dry miombo woodland differed with that for wet dry miombo woodland (Fig. 8a). This difference is due to the differences in species composition and distribution at each site. Furthermore, there are differences in soil type, soil moisture, temperature, nutrients, rainfall, and canopy closure at the two sites (i.e., Chidumayo, 2001; Fuller, 1999). However, temporal variations in the mean of aggregated LAI and NDVI values across different phenophases of the miombo woodland at the two sites were similar (r = 0.78, 0.76 for LAI and NDVI respectively) (Fig. 8c). Highest mean LAI and mean NDVI, both in the dry miombo woodland and wet miombo woodland, were observed in the maturity/peak phenophases during the mid-rainy season (January – March) (Figs. 5, 7i & 8c and Fig. A3 in the supplementary data).
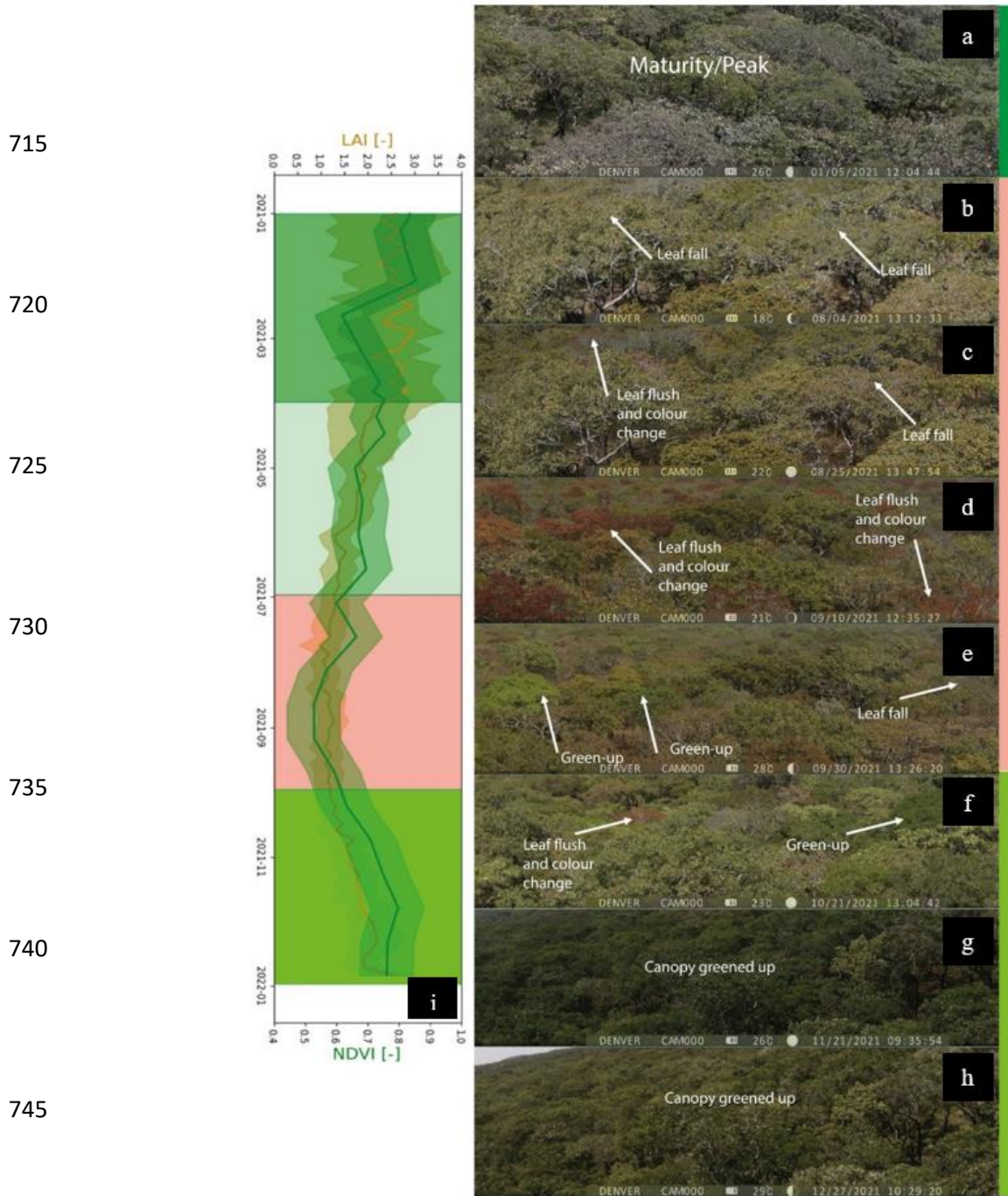
Figure 7: The wet miombo woodland canopy display trend for the year 2021 at Mpika study site (Lat: 12.387454°S; Long: 31.170911°E): (a) 5th January; (b) 4th August; (c) 25th August; (d) 10th September; (e) 30th September; (f) 21st October; (g) 21st November; and (h) 27th December. Shaded area are phenophases: January – March is the maturity/peak; April-June is the senescence/green-down; July-September is the dormant while October – December is the green-up/mid-greenup. (i) Temporal dynamics of MODIS LAI, NDVI (Shaded area for variables is the minimum and maximum). Emphasis was placed on the dormant and the green-up/mid-greenup phenophases when major changes in canopy display occurs.
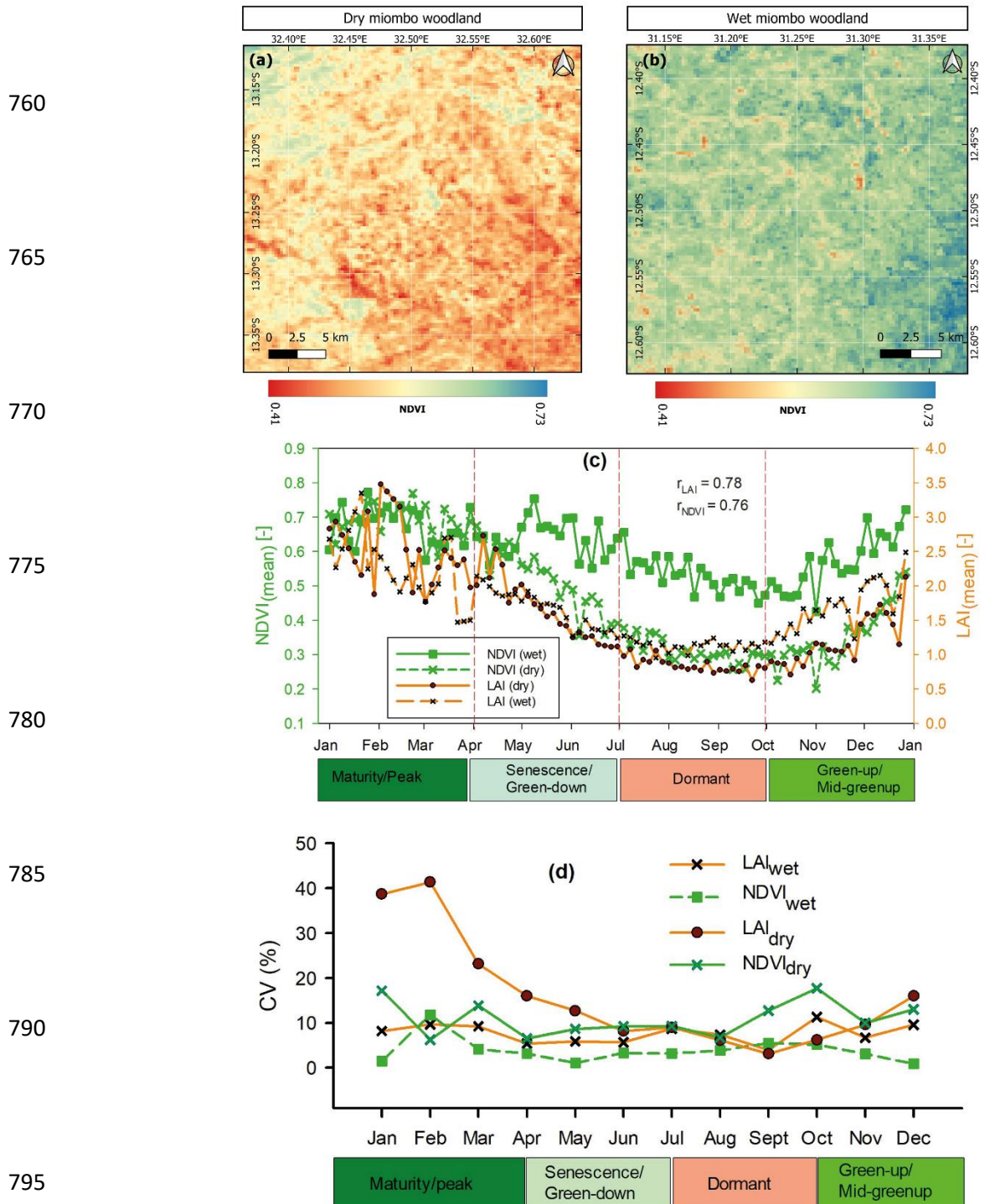
Figure 8: Spatial distribution of mean NDVI at the (a) dry miombo woodland and (b) wet miombo woodland site for the period January-December, 2021. (c) Temporal distribution of the mean of the aggregated LAI values and aggregated NDVI values for the wet miombo woodland and dry miombo woodland. (d) Temporal coefficients of variation in the mean LAI and NDVI values at the wet miombo woodland and dry miombo woodland in the Luangwa Basin in Zambia for the year 2021.

The maturity/peak period corresponds to the peak LAI and NDVI (Figs. 7 & 8), as noted by Chidumayo (2001). According to Chidumayo (2001), the miombo woodland experiences the highest green biomass between January and May. On the contrary, the dormant phenophase in August/September, which occurs during the warm pre-rainy season, exhibited the lowest LAI and NDVI values (Figs. 5, 7 & 8). This period is characterised by leaf-fall, leaf-flush, and changes in leaf colour (Figs. 7 & 9, Chidumayo, 2001; Chidumayo and Frost, 1996; Fuller, 1999).
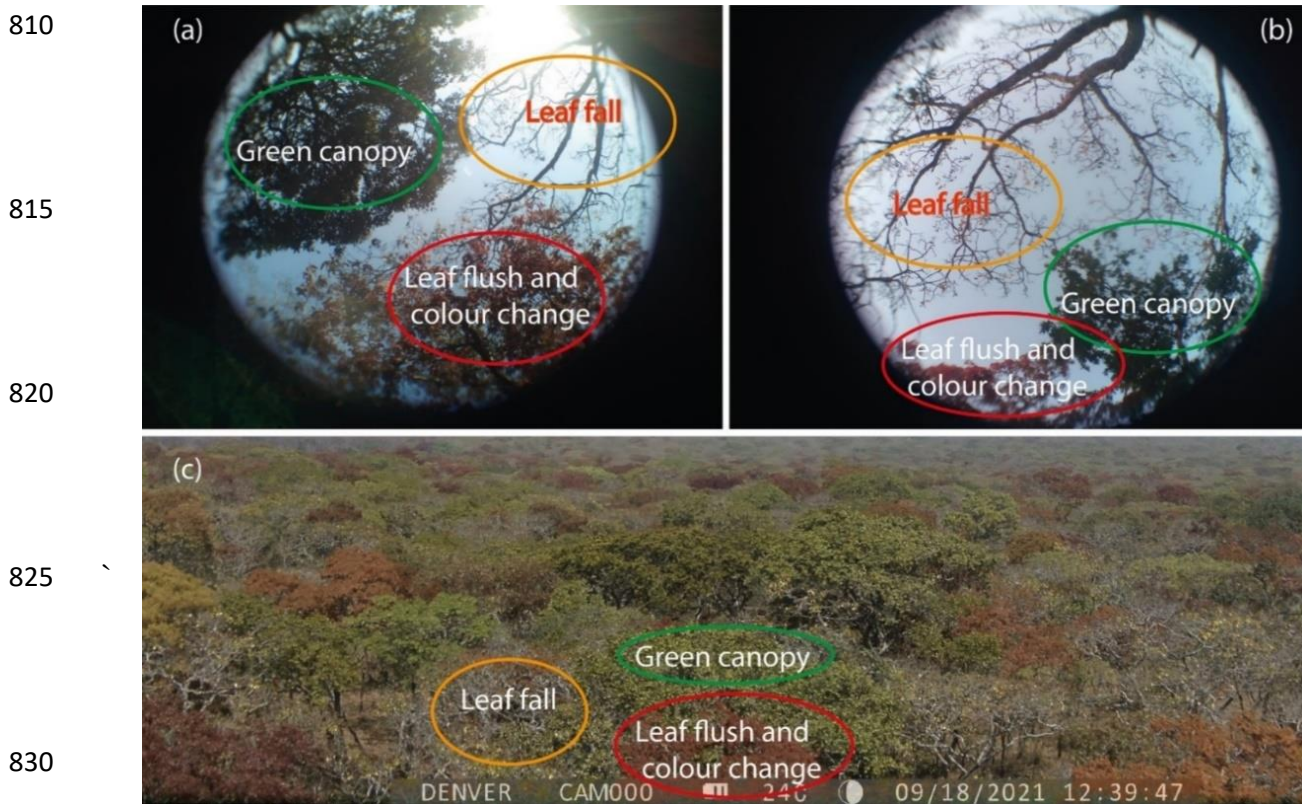
Figure 9: Heterogeneity in leaf-fall and leaf-flush activities among miombo woodland species: observed from under the canopy (a, b) and as observed above the canopy (c). Images taken at the wet miombo woodland site (Lat: 12.387454°S; Long: 31.170911°E) in Mpika, Zambia. Images taken on 18 September, 2021.

Table 2 presents the correlation coefficients for the temporal coefficients of variation of within-month variations in the means of the aggregated NDVI and LAI values for the dry miombo woodland and wet miombo woodland. The only period in which both LAI and NDVI values had significantly higher correlation coefficients (r = 0.97 for LAI and r = 0.75 for NDVI) in the temporal coefficients of variation for the dry miombo woodland and wet miombo woodland is the dormant phenophase (Fig. 8 and Table 2). This similarity in the coefficients of variation can be attributed to the plants undergoing similar phenological processes, such as leaf-fall and leaf-flush, during the dormant phase. During this phase, the grass component dries out, leaving only the tree component (i.e., the canopy) to determine the leaf area (Chidumayo, 2001). The increased temporal variations in NDVI values in August-September (Figs. 8d and 9) may also be explained by intensified leaf-fall, leaf-flush, and leaf colour changes. Increased leaf-fall activity can account

for the temporal coefficients of variation in mean LAI values in July and August over the wet miombo woodland (Figs. 8 and 9).

850

Table 2. Correlation coefficients (alpha value = 0.05) of the temporal coefficients of variation values of the within-month variations in the means of aggregated LAI and NDVI for the dry miombo woodland and wet miombo woodland.

	Dormant				Green-up/Mid-greenup			
	LAI_{wet}	$NDVI_{wet}$	LAI_{dry}	$NDVI_{dry}$	LAI_{wet}	$NDVI_{wet}$	LAI_{dry}	$NDVI_{dry}$
LAI_{wet}	1.00				1.00			
$NDVI_{wet}$	-1.00	1.00			0.35	1.00		
LAI_{dry}	0.97	-0.98	1.00		-0.19	-0.99	1.00	
$NDVI_{dry}$	-0.75	0.75	-0.59	1.00	0.96	0.59	-0.45	1.00

	Maturity/Peak				Senescence/Mid-Greendown			
	LAI_{wet}	$NDVI_{wet}$	LAI_{dry}	$NDVI_{dry}$	LAI_{wet}	$NDVI_{wet}$	LAI_{dry}	$NDVI_{dry}$
LAI_{wet}	1.00				1.00			
$NDVI_{wet}$	0.87	1.00			-0.86	1.00		
LAI_{dry}	-0.10	0.40	1.00		-0.38	-0.14	1.00	
$NDVI_{dry}$	-0.90	-1.00	-0.35	1.00	0.73	-0.27	-0.91	1.00

855

Fuller (1999) observed that in the wet miombo woodland, the co-occurrence of leaf-fall and leaf-flush in August and September, as shown in Fig. 9, resulted in a net-zero change in canopy closure. This net-zero change increase in canopy closure may explain the low temporal coefficient of variation of mean LAI values in September (Fig. 8d). The high temporal coefficients of variation
860   in the mean of the aggregated LAI and NDVI values for both the dry and wet miombo woodland during the maturity/peak phenophase (Fig. 8d) in the mid-rainy season can be attributed to two factors: heterogeneous growth of the green biomass of the woodland, occurring between January and May (Chidumayo, 2001; Fuller, 1999), and the influence of cloud cover on the quality of satellite-based LAI and NDVI products (Vermote and Wolfe, 2015; Zang et al., 2003).
865   Furthermore, differences in canopy closure between the dry miombo woodland and wet miombo woodland (Fuller, 1999) may contribute to variations in the temporal coefficients of variation in the mean of the aggregated LAI and mean NDVI values during the maturity/peak and senescence/green phenophases. For example, the dry miombo woodland, which has a lower canopy closure compared to the wet miombo (Fuller, 1999), is likely to have a higher grass
870   component. Additionally, differences in miombo species composition, distribution of rainfall, soil type, and soil moisture, among other variables, may result in varied phenological differences between the dry miombo woodland and wet miombo woodland (Chidumayo, 2001; Fuller, 1999).
Overall, the results of the ANOVA (see Fig. A9 and Table A2 in the supplementary data) indicate that there is no significant difference between the means of each satellite-based
875   evaporation estimate for the dry miombo woodland and wet miombo woodland. Consequently, further analyses used in this study for each satellite-based evaporation estimate are an average for the dry miombo woodland and wet miombo woodland in the Luangwa Basin (i.e., simply classified as miombo woodland in the Luangwa Basin).

3.3 Phenophase-based difference in satellite-based evaporation estimates

3.3.1 Deseasonalised time series, evaporation trend and evaporation anomalies

The original time series and the deseasonalised time series for the Luangwa Basin miombo woodland, dry miombo woodland, and wet miombo woodland are displayed in Fig. A4.1, Fig. A4.2 and Fig. A5 in the supplementary data. The temporal monthly anomalies of the means of evaporation, LAI and NDVI are presented in Figure 10.

The deseasonalised time series exhibits diverse temporal dynamics and magnitudes in satellite-based evaporation estimates for both dry miombo woodland and wet miombo woodland for the period 2009 to 2020 (Figs. A4.1 & A4.2 in the supplementary data).

The Mann-Kendall trend analysis reveals different degrees of decline in deseasonalised evaporation estimates by FLEX-Topo, GLEAM, SSEBop, and WaPOR (Kendall's tau > -0.1, p-value < 0.05). Conversely, MOD16A2 and TerraClimate demonstrate no discernible trend (refer to Table A3 in the supplementary data).

Overall, the evaporation anomalies, LAI anomalies and NDVI anomalies (Fig. 10 a) suggest that differences in the satellite-based evaporation estimates vary depending on the phenophase with more nuanced variations pronounced in the dormant phenophase in the dry season. There also seem to be two peaks in evaporation during the green-up/mid-greenup and maturity/peak phenophases. Similar peaks in LAI and NDVI are also observed during the same periods, which indicates a positive correlation between canopy cover and evaporation. However, this relationship does not seem to hold true during the dormant phenophase in the dry season (Fig. 10). Although the MOD16A2 and TerraClimate estimates show contrasting temporal dynamics and higher evaporation values, the rest of the satellite-based evaporation estimates appear to have similar temporal pattern during the green-up/mid-greenup and maturity/peak phenophase in the rainy season.
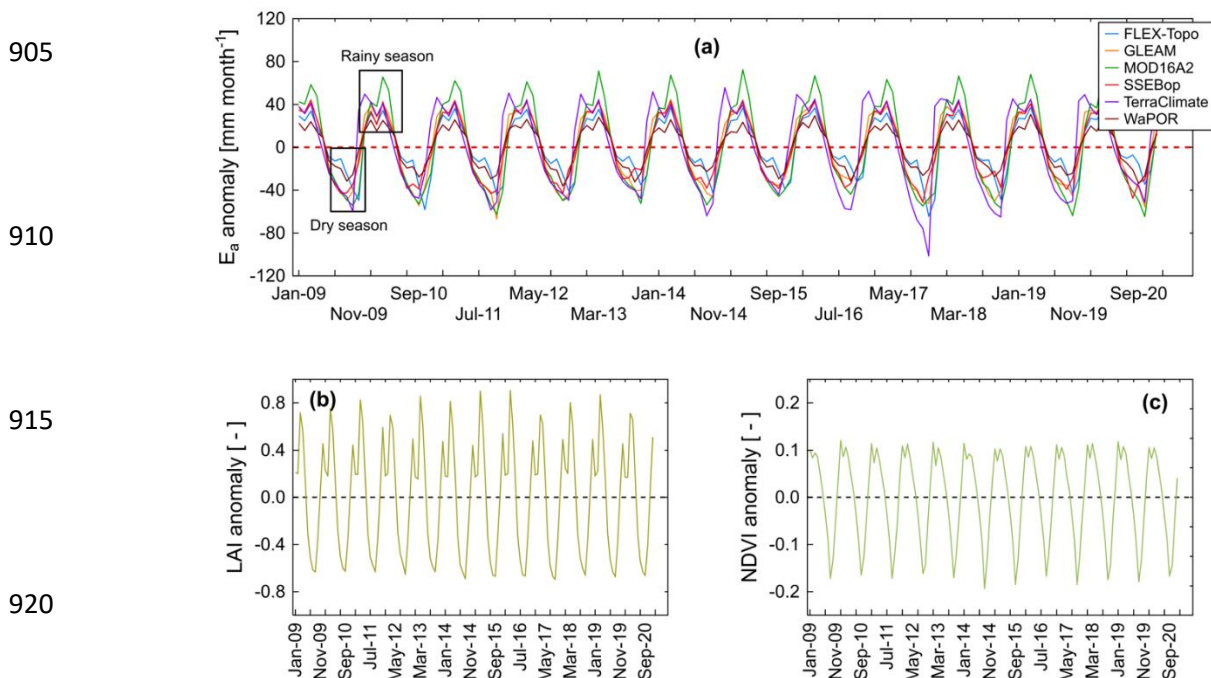
Figure 10. Temporal monthly anomalies of the mean satellite-based evaporation estimates (a), monthly anomalies of mean LAI (b) and monthly anomalies of mean NDVI (c) time series for the miombo woodland in the Luangwa Basin.

These discrepancies in deseasonalised time series, trends and monthly anomalies reveals the divergent temporal dynamics in satellite-based evaporation estimates in the miombo woodland within the Luangwa Basin.

The following sections provide detailed analyses of the anomalies and deseasonalised data based on phenophases. (phenophases are shown in Fig. 2 and as described in Section 2.2.1).

3.3.2 Temporal distribution and correlation of satellite-based evaporation estimates

Figure A3 in the supplementary data shows the temporal distribution of evaporation in relation to the proxy of woodland canopy cover (i.e., NDVI) and rainfall across phenophases in a hydrological year of the Luangwa Basin. The highest temporal mean satellite-based evaporation estimates were observed in the maturity/peak phenophase during the rainy season (with highest NDVI values) while the lowest were in the dormant phenophase in the dry season (with lowest NDVI values) (Fig. A3 in the supplementary data). With reference to original time series, deseasonalised time series, and monthly time series of anomalies, in different phenophases, each satellite-based evaporation estimate appeared to correlate differently with other evaporation estimates (Figs. 11, 12 and Figs. A5 – A8 in the supplementary data).
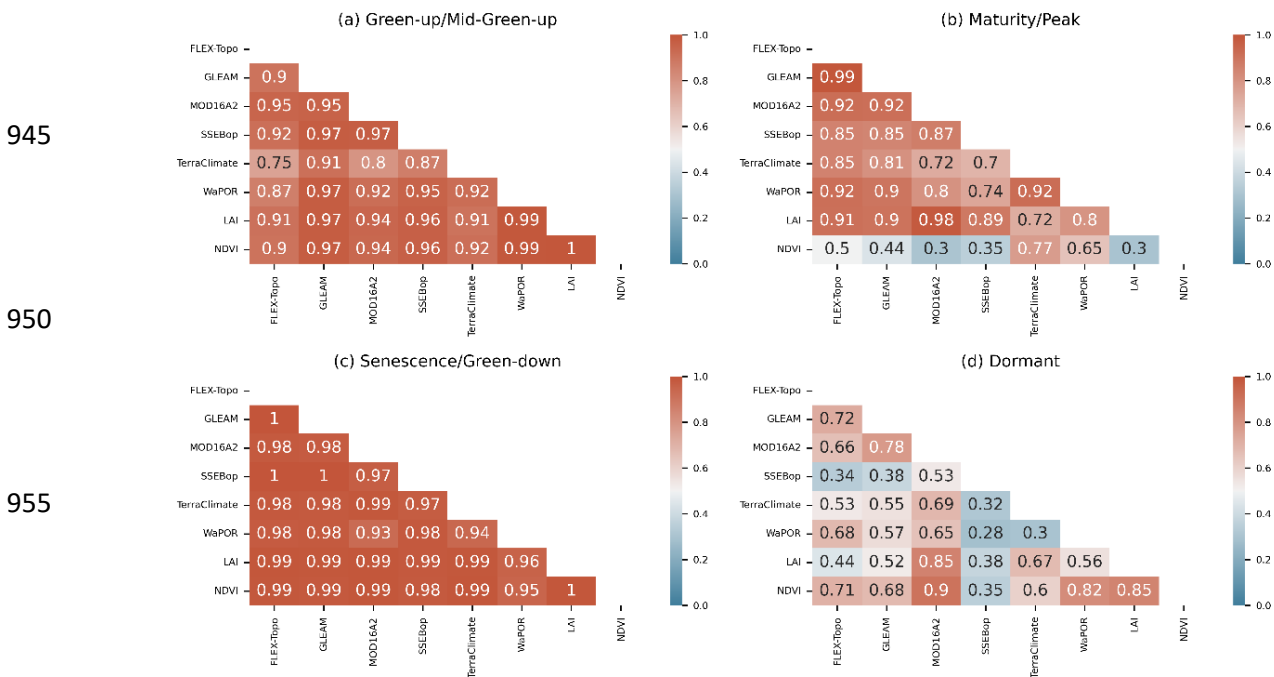
Figure 11. Temporal correlation of monthly anomalies of mean satellite-based evaporation estimates, mean LAI and mean NDVI in the miombo woodland, Luangwa Basin, Zambia. (a) green-up/mid-greenup phenophase, (b) maturity/peak phenophase, (c) senescence/green-down phenophase, and (d) dormant phenophase.

A correlation analysis of the means of the temporal time series showed significantly stronger correlation coefficients ($r > 0.5$, p-value < 0.05) among the satellite-based evaporation estimates during the transition periods in the green-up/mid-Greenup and senescence/mid-green down phenophases (Figs, 11 & 12). On the contrary, significantly weaker ($r < 0.5$, P-value < 0.05)

correlations were observed during the dormant phenophase in the warm dry season (Figs. 11,12 and Figs. A5 - A8 in the supplementary data). Stronger correlations of the temporal satellite-based evaporation estimates appear to occur during periods with high woodland leaf area, high soil moisture content, and high vegetation water during transition periods into the rainy season and into the dry season (Figs. 5, 7, 11, 12).
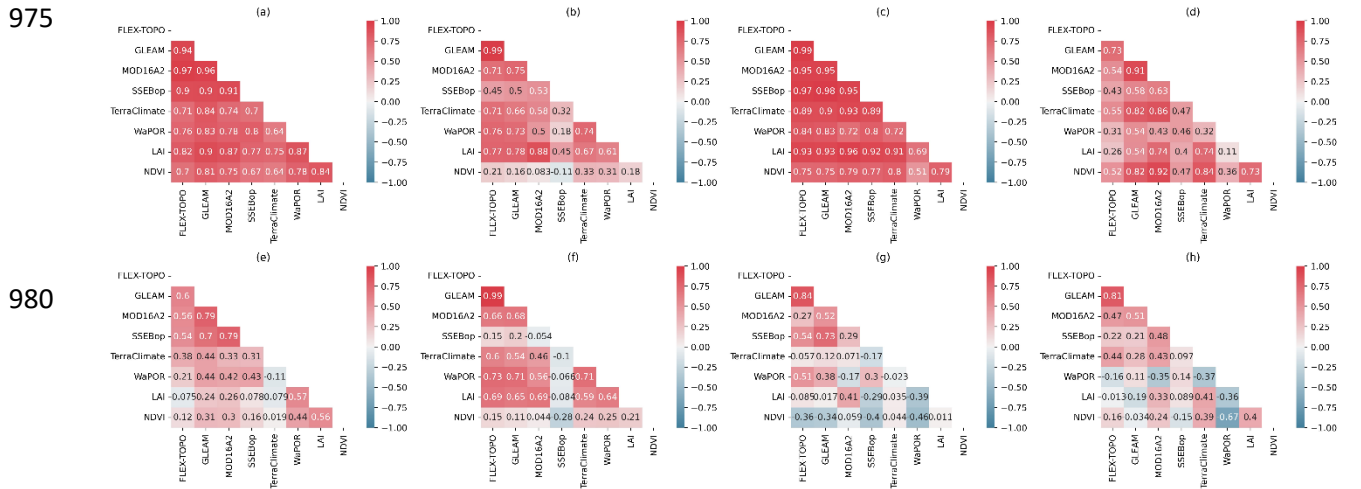
Figure 12. Temporal correlation of the monthly means of satellite-based evaporation estimates and proxies (LAI and NDVI) for woodland canopy cover for the miombo woodland in the Luangwa Basin across satellite-based phenophases: (a-d) original time series, (e) – (h) deseasonalised time series. (a, e) green-up/mid-green-up, (b, f) maturity/peak, (c, g) senescence/green-down/mid-green-down, (d, h) dormant.

On the other hand, the lowest temporal correlation coefficients among satellite-based evaporation estimates appear to occur during periods of water stress in the warm dry season (Figs. 5, 7, 11, 12 & 13). Generally, compared to original time series, the deseasonalised time series yielded lower coefficients of correlation among the satellite-based evaporation estimates across seasons and phenophases (Figs. 12 & 13) and highlight the significance of deseasonalising and removing trend from time series for a better understanding of real correlations. The same pattern in the temporal correlation of the satellite-based evaporation estimates observed for the miombo woodland at the Luangwa Basin scale was also observed for both the dry miombo woodland and the wet miombo woodland (Figs. A5 – A8 in the supplementary data).

3.3.3 Temporal variations in satellite-based evaporation estimates across phenophases
Original time series and deseasonalised time series of satellite-based evaporation estimates

A comparison of the aggregated means of the satellite-based evaporation estimates from 2009 to 2020 showed that the temporal coefficients of variation (CVs) for the original time series (Fig. 13 a-d) were larger, while the CVs for the deseasonalised time series (Fig. 13 e-h) were lower, between phenophases (see Figs. 13). This finding further emphasises, as mentioned above, the importance of eliminating seasonality and trend from time series when assessing long term relationships among variables.
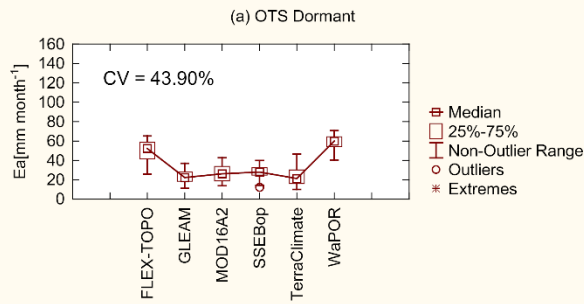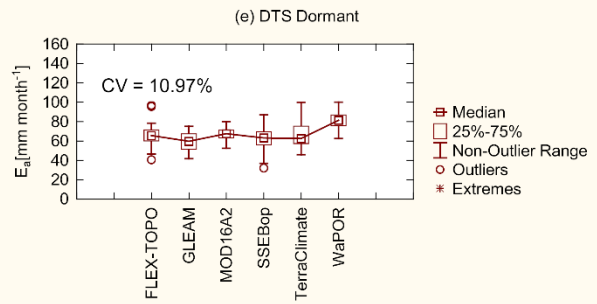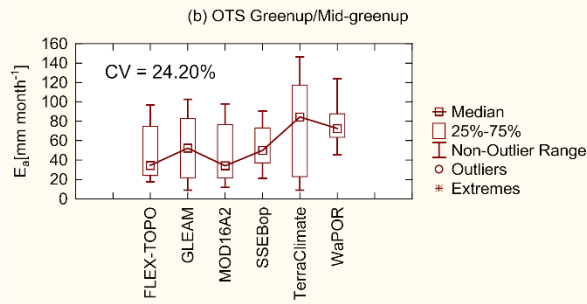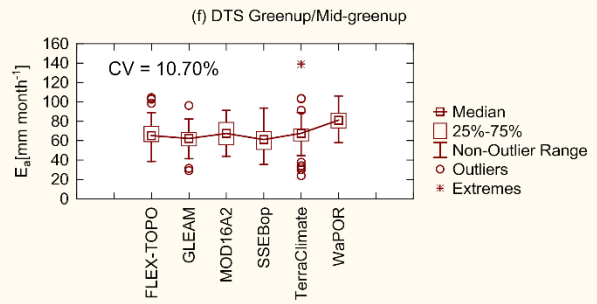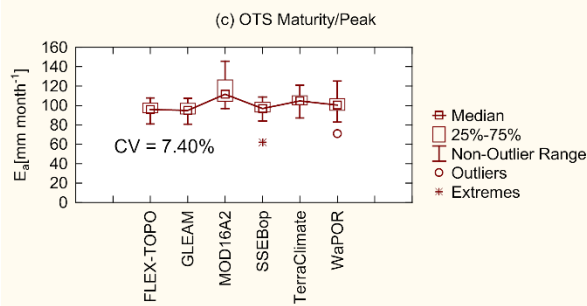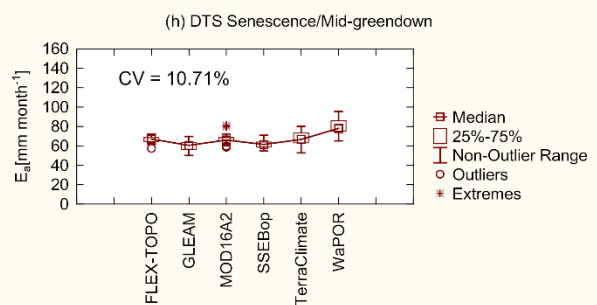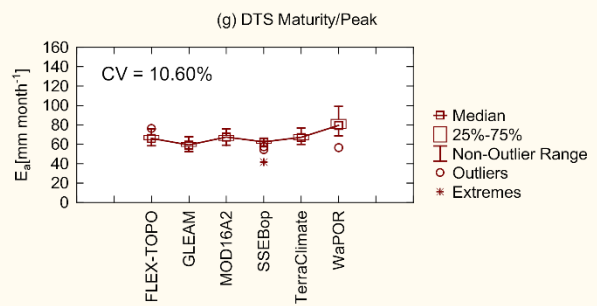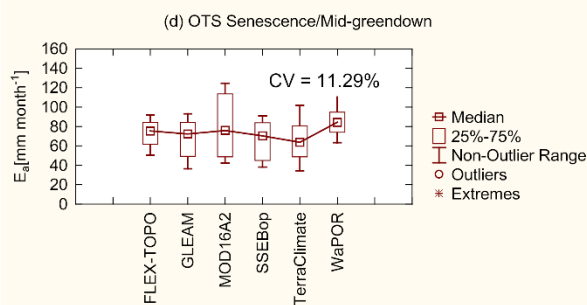
Figure 13: Box plots comparing satellite-based evaporation estimates, (a-c) original time series (OTS) and (c-f) with deseasonalised time series (DTS), across phenophases of the miombo woodland for the period 2009 - 2020 in the Luangwa Basin. The temporal coefficient of variation (CV) is for the comparison between the six satellite-based evaporation estimates.

Phenophases and coefficients of variation of satellite-based evaporation estimates

The higher temporal coefficient of variation in the means of satellite-based evaporation estimates (43.90%, 10.97% for original time series (a) and deseasonalised time series (e), respectively) shows that there are significant differences in the amounts of evaporation estimates

during the dormant phenophase (Figs. 13 & Fig. A9 in the supplementary data). This indicates that the adapted phenological and physiological attributes of the miombo species, may play a role in regulating evaporation during the dormant phenophase in the dry season. The CV from the comparisons of the temporal means of satellite-based evaporation estimates increase during this period because it is when the most changes occur in phenology, such as the co-occurrence of leaf fall and leaf flush (i.e., changes in LAI), as well as changes in leaf colour (i.e., changes in NDVI). This is also the driest period of the year with rising temperatures, during which adapted physiological characteristics, such as accessing groundwater, likely come into play to withstand the dry season conditions. Therefore, there are differences in how satellite-based estimates account for these changes in climate variables and phenological changes, resulting in the observed high CVs. Additionally, the CVs from the comparison of the monthly estimates for each satellite-based estimate (Table A4 in the supplementary data) shows higher CVs in the dormant phenophase which is probably due to reduced soil moisture and the changes in the woodland canopy as a result of the leaf-fall and leaf-flush that affects the surface area for evaporation.

The green-up/mid-greenup phenophase is a transition phenophase between the dry season and rainy season. An almost half reduction in the CV was observed from 43.90% in the dormant phenophase to 24.3% in the green-up/mid-greenup phenophase. The green-up/mid-greenup phenophase is at the start of the rainy season with increasing LAI and high canopy cover (i.e., mean NDVI between 0.5 and 0.7) and highest net radiation (i.e., 150 Wm^{-2}) (Figs. 5, 7 & 8). The increasing woodland canopy cover (i.e., LAI) and soil water conditions due to rainfall activity probably reduces the uncertainty in evaporation assessment as can also be evidenced by the increased temporal correlation coefficients between the satellite-based evaporation estimates (Fig. 11a & 12a). In Table A4 in the supplementary data the green-up/mid-greenup phenophase showed the largest CVs of satellite-based evaporation estimates. This is probably due to both the continued changes in the woodland canopy cover which affect the evaporative surface area and the commencement of rainfall activities resulting in temporal variations in evaporation (Figs. 5, 7 & 8).

The maturity/peak phenophase in the rainy season showed the least CV, 7.40% for original time series and 10.60% for deseasonalised time series between the satellite-based evaporation estimates. The lower CVs are indicative of reduction in differences in the means of satellite-based evaporation estimates during periods with high woodland cover and high soil moisture content. Table A4 in the supplementary data also shows lowest CVs of each satellite-based evaporation estimate during the maturity/peak phenophase. This is probably as a result of an established uniform woodland canopy cover when there is no leaf-fall and leaf-flush providing a stable evaporative surface. Additionally, consistent rainfall activity and soil moisture would have been attained by this period therefore not causing significant variations in the evaporation (Figs. 5, 7 & 8).

The senescence/green-down is a transition phenophase between the rainy season and dry season. During this phenophase, the differences in the means of satellite-based evaporation are low relative to the dormant phenophase (CV = 11.29% and 10.71% for original time series and deseasonalised time series, respectively). However, relative to the maturity/peak phenophase, they indicate the beginning of an increase in differences in the means of satellite-based evaporation estimates. Table A4 in the supplementary data show high CVs for each satellite-based estimate, relative to the maturity/peak phenophase, as variations in rainfall increase and soil moisture begins to decrease (Figs. 5, 7 & 8).

3.3.33 Satellite-based evaporation estimates and phenology of the miombo woodland in the dry season

In the dormant phenophase in the warm dry season the WaPOR, followed by FLEX-Topo, showed higher estimates of evaporation compared to other satellite-based evaporation estimates (Figs. 13 & Tables A4, Fig. A9 in the supplementary data). Zimba et al. (2023) showed, at point scale in the wet miombo woodland, that satellite-based evaporation estimates (FLEX-Topo, GLEAM, MOD16, SSEBop, TerraClimate and WaPOR) underestimated actual evaporation in the warm dry season. They also showed that while the NDVI was generally in a downward trajectory from May to September, the observed actual evaporation estimates had a rising trajectory which was in agreement with the rising air temperature and net radiation. Compared to other satellite-based estimates the WaPOR followed the same temporal dynamics as the field observations of actual evaporation of the wet miombo woodland in the dry season (Zimba et al., 2023). In this study, WaPOR showed negative correlation with the LAI/NDVI in the warm dry season/dormant phenophases (Figs. 12 g, h). Therefore, with reference to findings by Zimba et al. (2023) and Fig. 12 (g, h), the WaPOR appear to have the correct temporal dynamics of actual evaporation of the miombo woodland in the cool dry season/ senescence/green-down and the warm dry season/dormant phenophases.

3.3.4 Spatial-Temporal distribution of satellite-based evaporation estimates across phenophases

Figure 14 shows spatial-temporal distribution of satellite-based evaporation estimates across different phenophases for the hydrological year 2019/2020. The comparison was based on the entire Luangwa Basin, including non-miombo woodland regions. Generally, the spatial distribution and detail of evaporation estimates are different, but, like the temporal variations, they are most pronounced in the dormant and green-up phenophases (Figs. 12, 13, 14 and Table A3 in the supplementary data). During periods of high soil moisture and high leaf area (i.e., Figs. 5 & 7), in the maturity/peak and senescence/green-down phenophases, the products are more in agreement. It can further be seen that during the dormant phenophase, all six evaporation estimates showed higher actual evaporation in wooded areas (Fig. 14) (refer to Fig. 1 b, c for the cover of the miombo woodland in the Luangwa Basin). Potential contributing factors to the observed differences in spatial-temporal distribution of satellite-based evaporation estimates are highlighted in section 3.5.
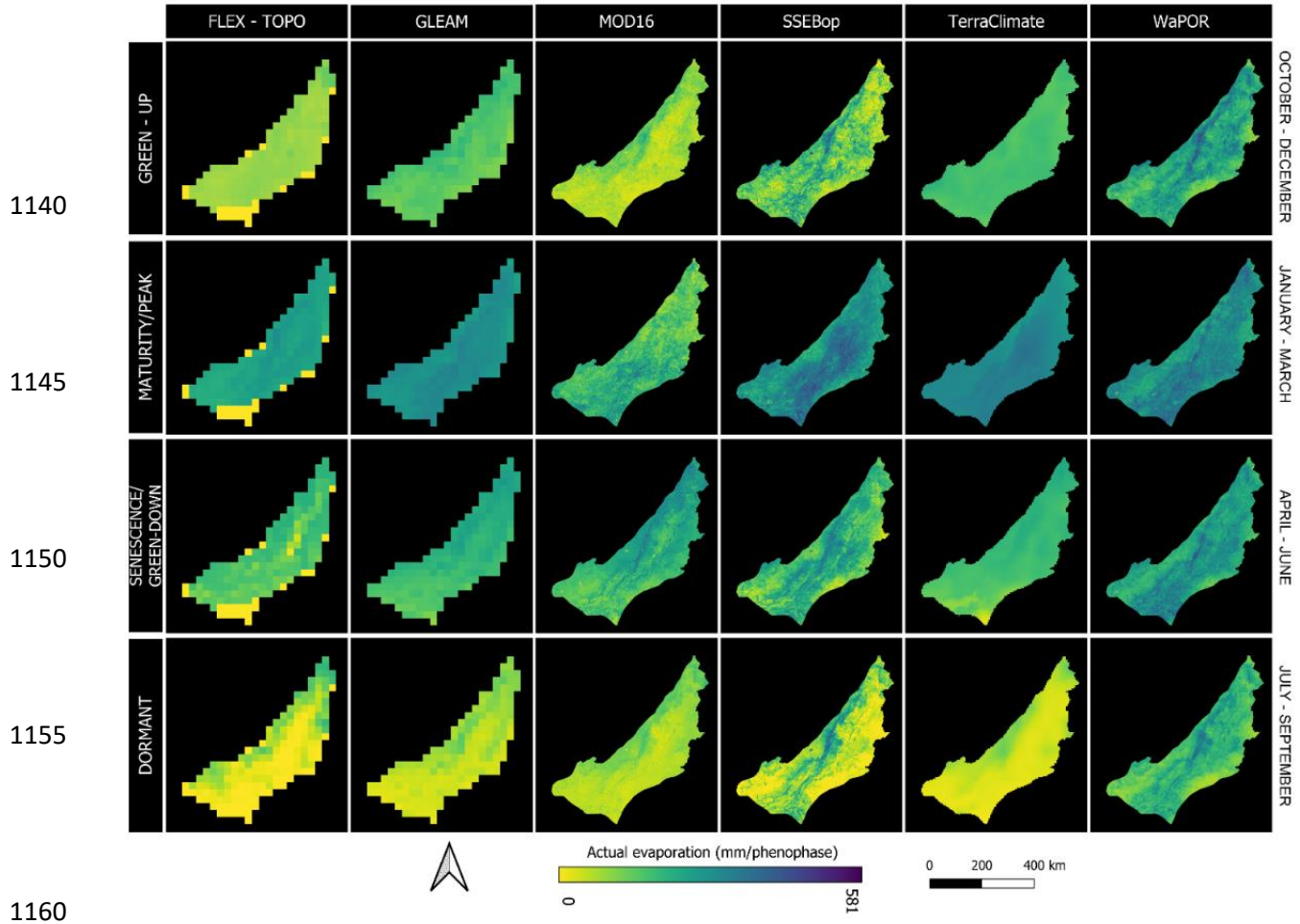
Figure 14: Spatial-temporal distribution of satellite-based evaporation estimates across different vegetation phenophases of the Luangwa Basin for the hydrological year September 2019 - August 2020.

3.3.5 Pairwise multiple comparison of satellite-based evaporation estimates at Luangwa Basin miombo woodland scale

As earlier indicated, there are no statistically significant differences in the mean estimates of evaporation for the dry miombo woodland and wet miombo woodland by each satellite-based evaporation estimate (Fig. A9 and Table A2 in the supplementary data). Therefore, the all pairwise comparison was performed only for the entire miombo woodland of the Luangwa Basin. Tables A5 and A6 in the supplementary data shows the results of the all pairwise multiple comparison of satellite-based evaporation estimates with seasonality (Table A5) and the deseasonalised time series (Table A6 in the supplementary data). For each phenophase (i.e., group) 33 monthly estimates (i.e., samples) of evaporation for each satellite-based estimate were used in the comparison. For both time series, it appeared the WaPOR estimates were the most different across phenophases (Fig. 15). The other satellite-based evaporation estimates with mean estimates significantly different from other estimates, after the WaPOR, are the FLEX-Topo, followed by the MOD16 and TerraClimate (Fig. 15, Tables A5 & A6 in the supplementary data).
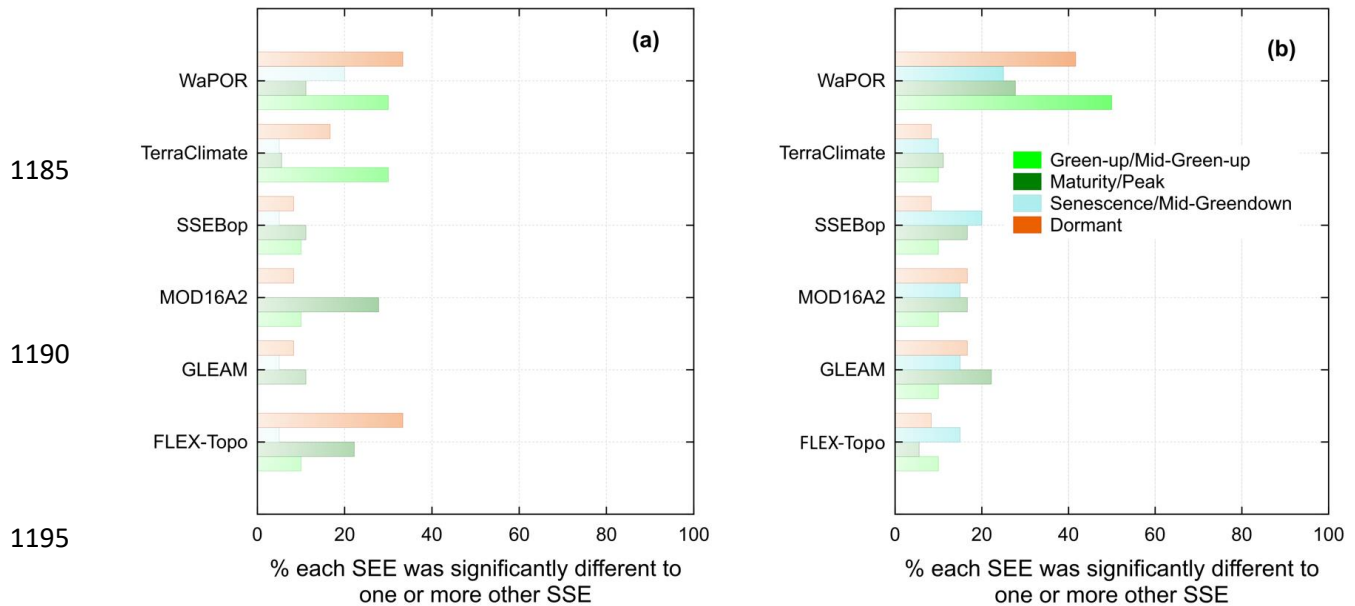
Figure 15: Percentage each satellite-based evaporation estimate (SEE) was significantly different to one or more other SSE in each phenophase at Luangwa Basin miombo woodland scale. (a) Comparison of satellite evaporation estimates original time series (OTS), and (b) Comparison of satellite evaporation estimates time series with deseasonalised time series (DTS).

3.3.5 Temporal variations in climate, LAI, NDVI and satellite-based evaporation estimates

With the exception of WaPOR, monthly temporal variations from the comparisons of the monthly means for each satellite-based evaporation estimates were highest during the green-up phenophase, followed by the dormant and senescence/green-down phenophases (Fig. 16). The maturity/Peak showed the lowest temporal coefficients of variations in the monthly means of each satellite-based evaporation estimates (Fig. 16 and Table A4 in the supplementary data).

The green-up and senescence/green-down phenophases are at the boundaries of the dry season into the mid-rainy season (in case of green-up phenophase) and the rainy season into the dry season (in the case of the senescence/green-down phenophase). The temporal coefficients of variation of the monthly means of NDVI (i.e., canopy cover), rainfall (i.e., water availability) and temperature (i.e., energy availability) in the green-up and senescence/green-down phenophases (Fig. 16) likely explains the temporal variations in the monthly means of each satellite-based evaporation estimates. The phenophases in which the means of LAI, NDVI, rainfall and soil moisture appear to show larger temporal coefficients of variations are also the phenophases in which the monthly means of individual satellite-based estimates show higher temporal coefficients of variation (Fig. 16).

The observed temporal coefficients of variation in the monthly means of each satellite-based evaporation estimates in the dormant phenophase could be as a result of the increase or reduction in the canopy cover due to the leaf-fall, leaf-flush and leaf-colour changes (i.e., NDVI as shown in Figs. 7, 8, 9 & 15). Figure 16 generally shows that the temporal variations in the means of the LAI, NDVI, rainfall, soil moisture and air temperature are mirrored in the temporal variations of the means of satellite-based evaporation estimates. As a result, satellite-based evaporation estimates are likely to exhibit significant variations due to weather conditions and year-to-year weather differences.
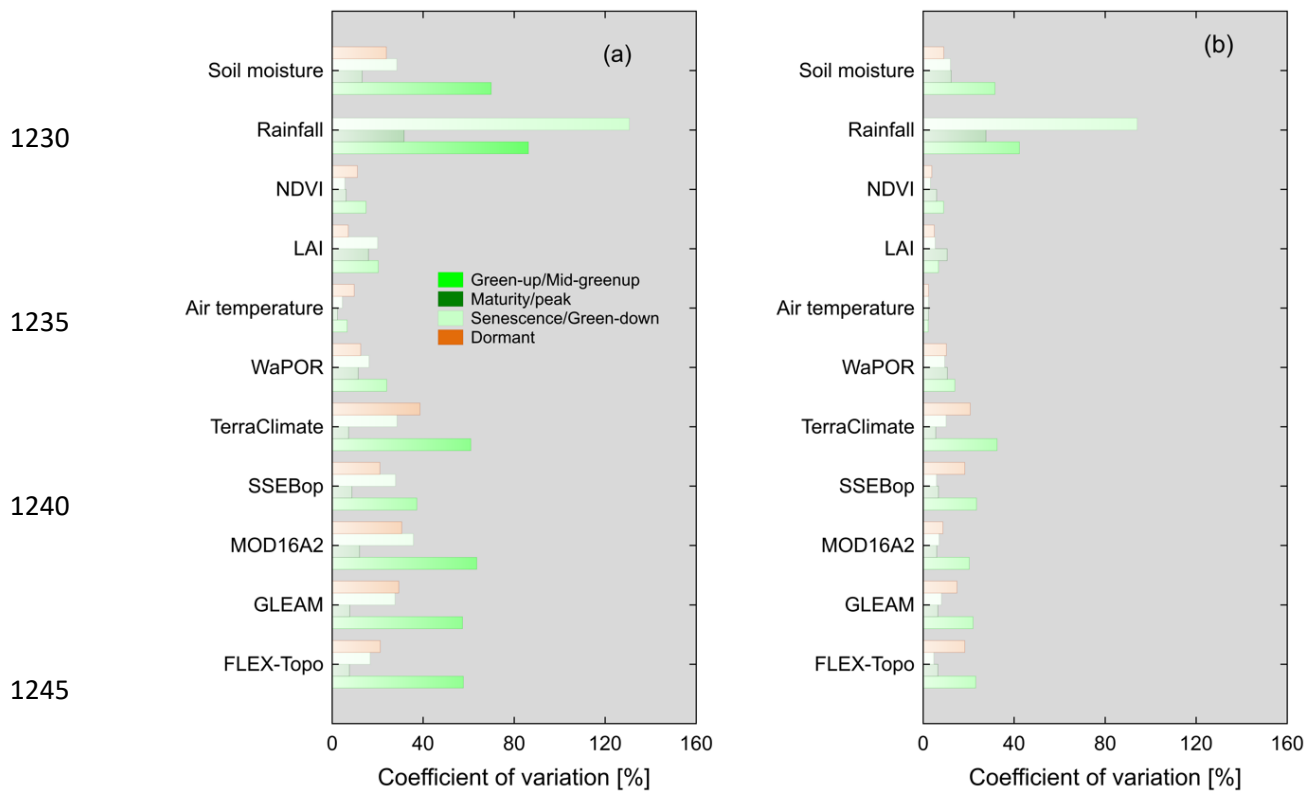
Figure 16: Temporal coefficients of variations in the means of variables for (a) original time series (OTS) and (b) deseasonalised time series (DTS) across phenophases for the miombo woodland, Luangwa Basin.

3.4 Comparison of satellite-based evaporation estimates to the water balance-based actual evaporation

Figure 17a compares satellite-based evaporation estimates with water balance-based actual evaporation estimates for the Luangwa Basin during the hydrological years from September 2009 to August 2020. This comparison included non-miombo woodland areas. Except for the FLEX-Topo (r = 0.55, p-value < 0.05) all other satellite-based evaporation estimates showed weak correlation (r < 0.5, *p-value* > 0.05) with the water balance-based actual evaporation (E_{wb}) (Fig. A10 and Table A7 in the supplementary data). Compared to the E_{wb} estimates, all six satellite-based evaporation estimates underestimated actual evaporation (Fig. 17, b). The poor correlation of the E_{wb} with satellite-based evaporation estimates can be due to several factors.

Firstly, the disregard of inter-annual storage may explain the very low actual evaporation estimate in the dry year 2015. In that year the over-year storage should likely not be disregarded, and it is also possible that farmers in the cropland areas withdrew water from small dams. Taking these factors into account would have led to a higher actual evaporation estimate in 2015. Secondly, the overall higher water balance-based actual evaporation may be due to the disregard of potential inter-basin groundwater exchange, or leakage of groundwater to the Zambezi. Hulsman et al. (2021) estimated that this leakage on average could amount to 143 mm y^{-1}. This amount would be enough to bridge the bias between WaPOR and the water balance-based actual evaporation in Fig. 17c.
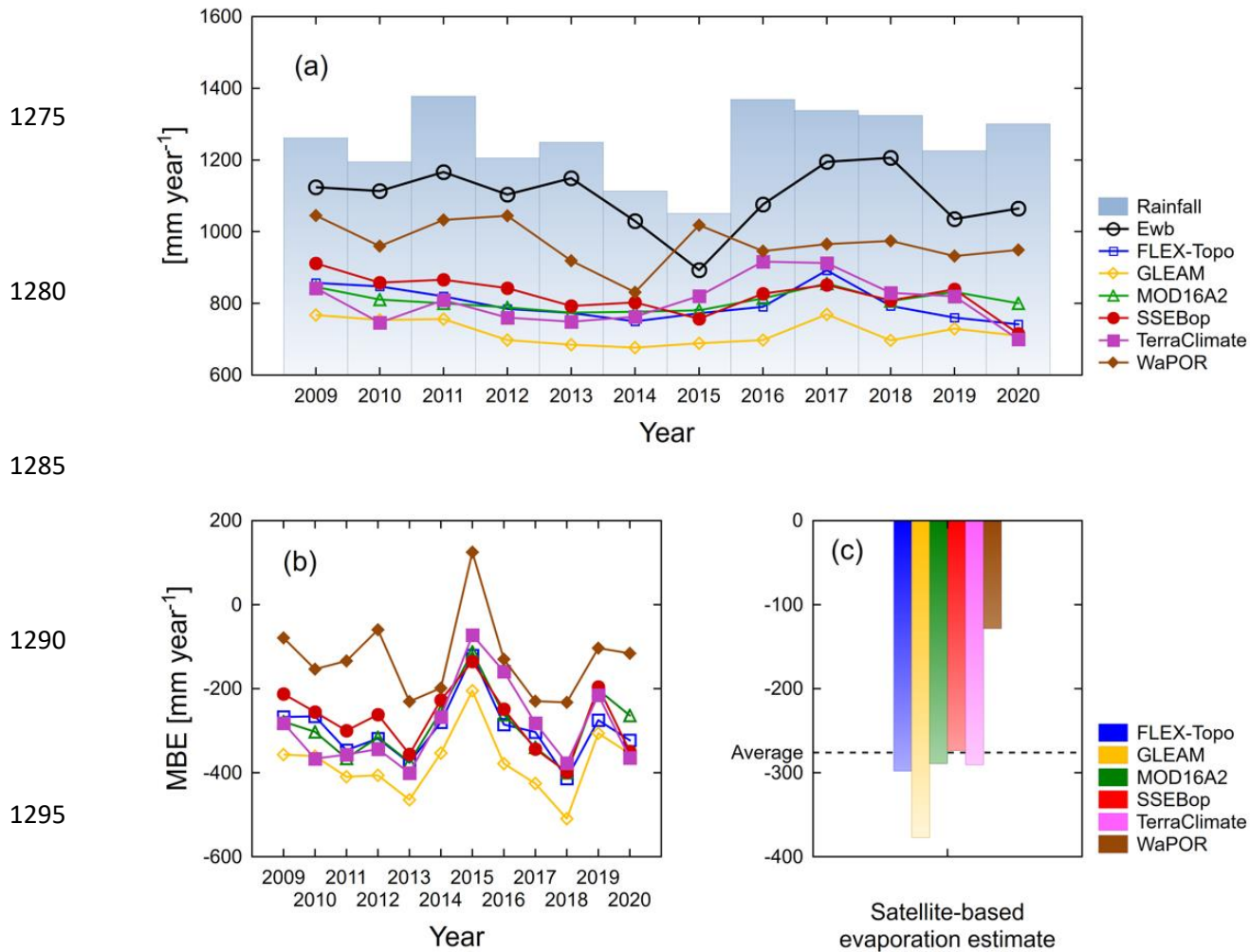
Figure 17: (a) Temporal comparison of satellite-based evaporation estimates to the water balance-based estimate of actual evaporation for the Luangwa Basin, and (b) comparison of the MBE of satellite-based evaporation estimates for each year, and (c) comparison of the multi-year average MBE of individual satellite-based evaporation estimates.

Furthermore, there are uncertainties in the river discharge and the spatially averaged precipitation, which may have been over-estimated. The extended runoff time series with TerraClimate (Fig. 4 c, d) may have been overestimated resulting in underestimating the water balance-based actual evaporation at basin scale. The assumption of overestimation of the extended runoff data is based on the validation results of the linear equation used to extend the runoff time series, which showed RMSE = 27 mm year^{-1} and MBE = 21 mm year^{-1}. In any given year, WaPOR appeared to have the least underestimation with an average MBE of 120 mm year^{-1}, while GLEAM had the largest underestimation with an average MBE of 370 mm year^{-1} (Fig. 17c).
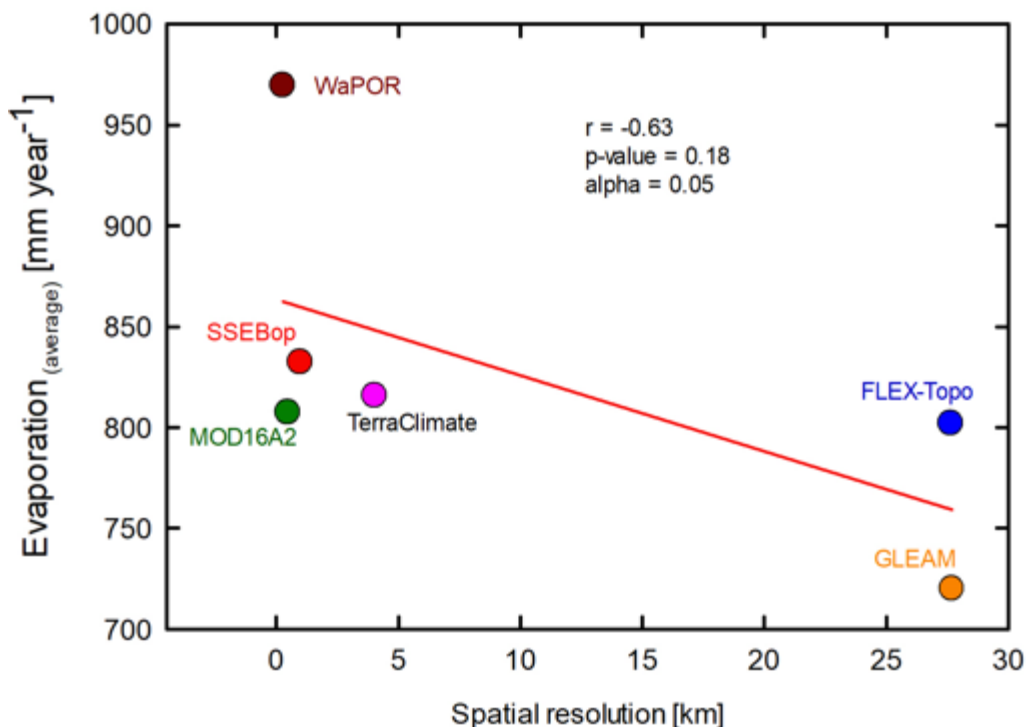
1330 Figure 18. Luangwa Basin scale relationship between 2009-2020 annual averages and spatial resolution of satellite-based evaporation estimates.

At basin scale, it appeared there was no statistically significant correlation (r = -0.63; *p-value* = 0.18; alpha = 0.05) between spatial resolution and evaporation estimates of each product (Fig. 18). For instance, TerraClimate, with a coarser spatial resolution, showed similar bias estimates as SSEBop and MOD16. MOD16 had an even higher spatial resolution than SSEBop, but underestimated more. FLEX-Topo had a coarser spatial resolution than MOD16 and SSEBop but exhibited higher estimates in the warm dry season/dormant phenophases (Fig. 14 and Fig. A3 in the supplementary data). The lack of a clear relationship between spatial resolution and actual evaporation estimates (Fig. 18), may imply that other factors such as the heterogeneity in the land cover (i.e., miombo woodland, mopane woodland, cropland, settlements etc), access to soil moisture and groundwater, differences in model structure (such as the inclusion of leakage), processes and model inputs, as highlighted in Zimba et al. (2023) and section 3.5 in this study, may be the largest contributing factors of the observed differences in the actual evaporation estimates at basin scale.

However, the underestimation of actual evaporation at basin scale by satellite-based evaporation estimates cannot be entirely attributed to the inaccuracies in the simulation of miombo woodland evaporation. The evaporation of other vegetation types, i.e., mopane woodland, has not been investigated. The basin scale water balance-based comparison suggests that satellite-based evaporation estimates possibly underestimate actual evaporation also in non-miombo woodland landscapes. This requires more investigation of different landscapes and land covers such as grassland, shrubland, wetland and mopane woodland. For a more comprehensive understanding of the evaporation of the Luangwa Basin there is need for the assessment of the interactions between

plant phenology and climate of each vegetation type and the accompanying potential influence on the evaporation dynamics of the basin. Nevertheless, the results of this study agreed with(Weerasinghe et al., 2020b) who showed that most satellite-based evaporation estimates generally underestimate evaporation across African basins (i.e., Zambezi Basin). The lower underestimation by WaPOR agreed with the point scale field observations for the wet miombo woodland (Zimba et al., 2023) and suggests that WaPOR is closest to actual evaporation of the miombo woodland in the Luangwa Basin.

3.5 Potential causes of differences in trends, magnitudes and spatial distribution of satellite-based evaporation estimates

Most pronounced differences in temporal dynamics and magnitudes of satellite-based evaporation estimates of the miombo woodland have been observed in the dormant phenophase of the dry season (Figs. 11-15 & Table A3 in the supplementary data). Evaporation during that period is dominated by transpiration (i.e., Tian et al., 2018). The dominant phenological characteristic of the miombo species in the dry season is the co-occurrence of leaf-fall, leaf-flush and greening up before commencement of seasonal rainfall (Figs. 7&9; Chidumayo and Frost, 1996; Frost, 1996) which affects transpiration (e.g., Marchesini et al., 2015; Snyder & Spano, 2013). Tian et al. (2018) showed that the terrestrial groundwater storage anomaly (TWS) continued to decrease throughout the dry season and was indicative that miombo trees used deep ground water during that period. The suggestion that miombo trees access ground water is supported by Savory (1963) who showed that miombo species are deep rooting beyond 5 m with capacity to access ground water. Therefore, it is likely that satellite-based evaporation estimates using models whose structure, processes and inputs take into account the highlighted interactions between plant phenology and climate during the dry season and early rainy season, especially the access to deep soil moisture, would produce more accurate trends and magnitudes of evaporation in the miombo woodland.

3.5.1 Use of proxies for soil moisture

Some studies have shown that direct integration of soil moisture rather than the use of proxies improves the accuracy of actual evaporation estimates (Brust et al., 2021; Novick et al., 2016). The challenge with the use of proxies for soil moisture, for example in surface energy balance models, is that these are unable to fully account for changes in other factors that may influence sensible heat fluxes (Gokmen et al., 2012). To improve the accuracy of estimation of water and energy fluxes in regions with recurrent plant water stress, such as in miombo woodland, Gokmen et al. (2012) suggested that the soil moisture be integrated in surface energy balance models. For instance, for MOD16 the use of the relative humidity and vapour pressure difference as proxies for soil moisture maybe a source of uncertainty in estimating transpiration (Novick et al., 2016). Direct integration of soil moisture into the MOD16 algorithm appeared to improve the accuracy of actual evaporation estimates (Brust et al., 2021). The energy balance-based SSEBop does not explicitly consider soil moisture dependency and assumes that the variations in satellite-based land surface temperature and vegetation indices, such as the NDVI, accounts for soil moisture (Senay et al., 2013). TerraClimate uses the plant-extractable water capacity of soil for soil moisture input. However, the difficulty in determining the plant-extractable water capacity of the soil is in defining the extent of the rooting depth. GLEAM takes into account 2.5m of the sub-surface linked to observed precipitation. On the other hand, transpiration in FLEX-Topo and WaPOR (ETLook model) is coupled to soil moisture in the root zone using an integrated approach. Consequently, this may explain why the pairwise comparison showed that trends and magnitudes

1400 of FLEX-Topo and WaPOR were not significantly (*p-value* > 0.05) different (in both dry miombo woodland and wet miombo woodland) during the dormant phenophase (Tables A5d in the supplementary data). Therefore, the integration of soil moisture in evaporation simulation and the accuracy of the soil moisture product used is likely to affect the accuracy of satellite-based transpiration estimates.

1405

3.5.2   Optimisation of the rooting depth

Optimising rooting depth rather than the use of a standard depth has been shown to increase transpiration of trees in landscapes with a dry season (Kleidon and Heimann 1998). Modifying rooting depth can improve energy flux simulations at both field scale and regional scale (Liu et al., 1410 2020). Wang-Erlandsson et al. (2016) showed that accurate root zone storage estimates "improved evaporation simulation overall, and in particular during the least evaporating months in sub-humid to humid regions with moderate to high seasonality". Their study demonstrated that several forest types have developed rootzone storage mechanisms that help buffering for dry season conditions. Some miombo species are deep rooting, beyond 5 metres, while the soil moisture in the miombo 1415 woodland increases with depth (i.e., Chidumayo, 2001; Savory, 1963). Additionally, the depth to ground water ranges between 0 – 25 mbgl for both wet miombo woodland and dry miombo woodland, although in a few places the range is between 25 – 50 mbgl (Bonsor and Macdonald, 2011). Therefore, one of the potential causes of the observed differences in satellite-based evaporation estimates could be the rooting depth used in the simulation of evaporation. The 1420 satellite-based evaporation estimates used in this study are likely not to have optimised rooting depth for the miombo woodland as there are few studies in the public domain that have conducted field-based investigations to determine the optimum rooting depth for effective simulation of transpiration of miombo woodland. Since ecosystems have adapted to local climatic conditions (Tian et al., 2018), global scale root storage estimates and optimisation may not be able to 1425 effectively capture the climatic conditions at local and region scales.

3.5.3   Differences in landcover products used

The landcover proxies in satellite-based evaporation estimates may also explain the observed differences in both temporal and spatial distribution of evaporation. For instance, the 1430 MOD16 uses a global landcover product (Gray et al., 2019) which had shown to misclassify certain land cover types and showed low user accuracy in certain regions (i.e., Leroux et al., 2014). WaPOR uses the Copernicus land cover product, but adds the distinction between irrigated and rain-fed areas (FAO, 2018). For the vegetation fraction, GLEAM uses MODIS MOD44B (Martens et al., 2017); (Miralles et al., 2011). Other satellite-based evaporation estimates (i.e., SSEBop) use 1435 vegetation indices such as the NDVI as proxy for vegetation cover.

Different vegetation types have different interactions between plant phenology and climate (i.e., Lu et al., 2006) which influence actual evaporation (Forster et al., 2022; Snyder & Spano, 2013; Schwartz, 2013). Transpiration of the miombo woodland in the dry season is dependent on the landcover type and constrained by: root zone water availability (Wang-Erlandsson et al., 2016; 1440 Gates and Hanks, 2015; Stancalie and Nert, 2012; Allen et al., 1998), stomatal conductance thresholds and surface roughness, which are vegetation type and plant species dependent (Urban et al., 2017); Wehr et al., 2017); Gates & Hanks, 2015; Tuzet, 2011). Therefore, dissimilarities in the land cover products and their associated limitations possibly reflect in differences in the spatial-temporal distribution of satellite-based evaporation estimates.

1445 ### 3.5.4   Satellite-based rainfall products and rainfall interception

The differences observed in evaporation estimates may be related to differences in the quality of satellite-based precipitation products used and the ability of the models to effectively account for rainfall interception. Studies have shown that satellite precipitation products are geographically biased towards either underestimation or overestimation (Macharia, Fankhauser, Selker, Neff, & Thomas, 2022;Asadullah, McIntyre, & Kigobe, 2008). In the case of Africa, and southern Africa in particular, no single precipitation product has been found to perform better than other precipitation products across landscapes (Macharia et al., 2022). The difference in precipitation products, with different spatial resolutions and accuracy levels, may explain the differences in the spatial-temporal distribution of satellite-based evaporation estimates during the rainy season. For instance, FLEX-Topo used the Climate Hazards Group Infra-Red Precipitation with Station data (CHIRPS) (Funk et al., 2015), GLEAM used Multi-Source Weighted-Ensemble Precipitation (MSWEP) (Beck et al., 2017) which uses different algorithms, inputs and spatial resolution. Rainfall interception is a function of vegetation cover, leaf area (LAI), spatial scale and precipitation. For instance, LAI influences canopy interception, throughfall and forest floor interception, and spatial and temporal scale influences the interception threshold (FAO, 2018; Gerrits, 2010; Savenije, 2004). Field observations showed that wet miombo woodland canopies intercepted up to 18-20 percent of rainfall annually (i.e., Alexandre, 1977). Therefore, differences in the quality and accuracy of land cover products, and even proxies such as the NDVI used for modelling interception, are likely to result in different evaporation estimates of evaporation products that have interception modules (i.e., FLEX-Topo, GLEAM, MOD16 and WaPOR).

4   Conclusions and recommendations

The study sought to find out to which extent a variety of satellite-based evaporation estimates were in agreement or differed in quantifying miombo woodland evaporation during its typical phenophases and to establish the underlying factor(s) for the discrepancies that emerged. The study also compared the different satellite-based evaporation estimates to the annual water balance-based evaporation at basin scale. The following were the conclusions:

Compared to the observed temporal dynamics in canopy display attributes of the wet miombo woodland in the dormant phenophase and the greenup/mid-green-up phenophase in the dry season (i.e., increase in leaf area (i.e., LAI) and the start in green-up (i.e., NDVI) in late September) only the WaPOR appear to follow the field observations of the changes in the plant phenology. Consequently, the WaPOR showed higher means of the aggregated estimates of evaporation than the other satellite-based evaporation estimates in the phenophases in the dry season.

Original time series, deseasonalised time series and the time series of anomalies appeared to show weaker temporal correlation coefficients and high temporal coefficients of variation in the means of aggregated satellite-based evaporation estimates in the dormant phenophase in the dry season. The observed differences in satellite-based evaporation estimates in the dormant phenophase in the dry season appear to be due to limited understanding and inadequate representation of the interactions between plant phenology and climate, that are influenced by the adapted physiological attributes such as the co-occurrence of leaf-fall and leaf-flush and the deep rooting of the miombo species with potential access to deep soil moisture including groundwater.

It is possible that the underestimations of satellite-based evaporation estimates, compared to the water-balance based evaporation estimates, are affected by the disregard of over year storage

in the deeper groundwater and the export of groundwater by leakage to the downstream Zambezi River. Another cause for the discrepancy is the inadequate representation of the plant phenology and climate interactions of the miombo species, but also of other vegetation types such as the mopane woodland. Consequently, field observations of evaporation across the different phenophases and strata of the miombo woodland are required to obtain a comprehensive overview of the characteristics of the actual evaporation of the ecosystem. This information can be used to help improve satellite-based evaporation assessments in the Luangwa Basin and the miombo region as a whole.

Finally, in view of the unique plant phenology, whereby the green-up and increase in the leaf area starts before the onset of rainfall, and the ability of the miombo species to access additional moisture stocks, inclusion of these traits is likely to improve satellite-based estimates of transpiration of the miombo woodland in the phenophases in the dry season.

Author contribution

Conceptualization, H.Z.; formal analysis, H.Z., P.H; resources, H.S.; supervision, M.C.-G. and B.K.; writing—original draft, H.Z.; writing—review and editing, M.C.-G., B.K., H.S., P.H., I.N., and N.V. All authors have read and agree to the published version of the manuscript.

Funding

This study was conducted with the financial support of the Dutch Research Council (NWO) under the project number W 07.303.102.

Acknowledgements

This study is part of the ZAMSECUR Project, which focuses on observing and understanding the remote water resources for enhancing water, food and energy security in Lower Zambezi Basin We wish to thank the Water Resources Management Authority (WARMA) in Zambia for the field discharge data used in this study.

Conflict of interest:

At least one of the (co-)authors is a member of the editorial board of Hydrology and Earth System Sciences.

References

Abatzoglou, J. T., Dobrowski, S. Z., Parks, S. A., and Hegewisch, K. C.: TerraClimate, a high-resolution global dataset of monthly climate and climatic water balance from 1958-2015, Sci Data, 5, 1–12, https://doi.org/10.1038/sdata.2017.191, 2018.

Abrams, M. and Crippen, R.: ASTER Global DEM (Digital Elevation Mode) - Quick Guide for V3, California Institute of Technology, 3, 10, 2019.

Alexandre, P. J.: Le bilan de l'eau dans le miombo (forêt claire tropicale), Bulletin de la Société géographique de Liège, 13, 107–126, 1997.

Allen, R. G., Pereira, L. S., Raes, D., and Smith, M.: FAO Irrigation and Drainage Paper No. 56 - Crop Evapotranspiration, FAO, Rome, 1–326 pp., 1998.

Asadullah, A., McIntyre, N., and Kigobe, M.: Evaluation of five satellite products for estimation of rainfall over Uganda, Hydrological Sciences Journal, 53, 1137–1150, https://doi.org/10.1623/hysj.53.6.1137, 2008.

1535 Auzmendi, I., Mata, M., Lopez, G., Girona, J., and Marsal, J.: Intercepted radiation by apple canopy can be used as a basis for irrigation scheduling, Agric Water Manag, 98, 886–892, https://doi.org/10.1016/j.agwat.2011.01.001, 2011.

Beck, H. E., Van Dijk, A. I. J. M., Levizzani, V., Schellekens, J., Miralles, D. G., Martens, B., and De Roo, A.: MSWEP: 3-hourly 0.25° global gridded precipitation (1979-2015) by merging
1540 gauge, satellite, and reanalysis data, Hydrol Earth Syst Sci, 21, 589–615, https://doi.org/10.5194/hess-21-589-2017, 2017.

Beilfuss, R.: A Risky Climate for Southern African Hydro ASSESSING HYDROLOGICAL RISKS AND A Risky Climate for Southern African Hydro, https://doi.org/10.13140/RG.2.2.30193.48486, 2012.

1545 Biggs, T., Petropoulos, G. P., Velpuri, N. M., Marshall, M., Edward, G. P., Nagler, Pamela., and Messina, A.: Remote Sensing of Evapotranspiration from Croplands, Remote Sensing of Water Resources, Disasters, and Urban Studies, 59–99, 2015.

Bogawski, P. and Bednorz, E.: Comparison and Validation of Selected Evapotranspiration Models for Conditions in Poland (Central Europe), Water Resources Management, 28, 5021–
1550 5038, https://doi.org/10.1007/s11269-014-0787-8, 2014.

Bonnesoeur, V., Locatelli, B., Guariguata, M. R., Ochoa-Tocachi, B. F., Vanacker, V., Mao, Z., Stokes, A., and Mathez-Stiefel, S. L.: Impacts of forests and forestation on hydrological services in the Andes: A systematic review, For Ecol Manage, 433, 569–584, https://doi.org/10.1016/j.foreco.2018.11.033, 2019.

1555 Bonsor, H. C. and Macdonald, A. M.: An initial estimate of depth to groundwater across Africa, 2011.

Briuinger, D. R., Krishnaiah, P. R., and Cleveland, W. S.: Seasonal and Calendar Adjustment, Handbook of statistics, 3, 39–72, 1983.

Brust, C., Kimball, J. S., Maneta, M. P., Jencso, K., He, M., and Reichle, R. H.: Using SMAP
1560 Level-4 soil moisture to constrain MOD16 evapotranspiration over the contiguous USA, Remote Sens Environ, 255, 112277, https://doi.org/10.1016/j.rse.2020.112277, 2021.

Buchhorn, M.; Smets, B.; Bertels, L.; De Roo, B.; Lesiv, M.; Tsendbazar, N.E., Linlin, L., Tarko, A.: Copernicus Global Land Service: Land Cover 100m: Version 3 Globe 2015-2019: Product User Manual, Zenodo, Geneve, Switzerland, https://doi.org/10.5281/zenodo.3938963, 2020.

1565 Cheng, M., Jiao, X., Li, B., Yu, X., Shao, M., and Jin, X.: Long time series of daily evapotranspiration in China based on the SEBAL model and multisource images and validation, Earth Syst Sci Data, 13, 3995–4017, https://doi.org/10.5194/essd-13-3995-2021, 2021.

Chidumayo, E. N.: Phenology and nutrition of miombo woodland trees in Zambia, Trees, 9, 67–72, https://doi.org/10.1007/BF00202124, 1994.

1570   Chidumayo, E. N.: Climate and Phenology of Savanna Vegetation in Southern Africa, Journal of Vegetation Science, 12, 347, https://doi.org/10.2307/3236848, 2001.

Chidumayo, E. N. and Gumbo, D. J.: The dry forests and woodlands of Africa : managing for products and services, Earthscan, 288 pp., 2010.

Cleland, E. E., Chuine, I., Menzel, A., Mooney, H. A., and Schwartz, M. D.: Shifting plant
1575   phenology in response to global change, Trends Ecol Evol, 22, 357–365, https://doi.org/10.1016/j.tree.2007.04.003, 2007.

Van Der Ent, R. J., Savenije, H. H. G., Schaefli, B., and Steele-Dunne, S. C.: Origin and fate of atmospheric moisture over continents, Water Resour Res, 46, 1–12, https://doi.org/10.1029/2010WR009127, 2010.

1580   Van Der Ent, R. J., Wang-Erlandsson, L., Keys, P. W., and Savenije, H. H. G.: Contrasting roles of interception and transpiration in the hydrological cycle – Part 2: Moisture recycling, Earth System Dynamics, 5, 471–489, https://doi.org/10.5194/esd-5-471-2014, 2014.

Fan, Y., Miguez-Macho, G., Jobbágy, E. G., Jackson, R. B., and Otero-Casal, C.: Hydrologic regulation of plant rooting depth, Proceedings of the National Academy of Sciences, 114, 10572–
1585   10577, https://doi.org/10.1073/pnas.1712381114, 2017.

FAO: WaPOR Database Methodology: Level 1 Data, 72 pp., 2018.

Forrest, J. and Miller-Rushing, A. J.: Toward a synthetic understanding of the role of phenology in ecology and evolution, Philosophical Transactions of the Royal Society B: Biological Sciences, 365, 3101–3112, https://doi.org/10.1098/rstb.2010.0145, 2010.

1590   Forrest, J., Inouye, D. W., and Thomson, J. D.: Flowering phenology in subalpine meadows: Does climate variation influence community co-flowering patterns?, Ecology, 91, 431–440, https://doi.org/10.1890/09-0099.1, 2010.

Forster, M. A., Kim, T. D. H., Kunz, S., Abuseif, M., Chulliparambil, V. R., Srichandra, J., and Michael, R. N.: Phenology and canopy conductance limit the accuracy of 20 evapotranspiration
1595   models in predicting transpiration, Agric For Meteorol, 315, 108824, https://doi.org/10.1016/j.agrformet.2022.108824, 2022.

Frost, P.: The Ecology of Miombo Woodlands, edited by: Campbell, B., Center for International Forestry Research, Bogor, Indonesia, 11–55 pp., 1996a.

Frost, P.: The Ecology of Miombo Woodlands, edited by: Campbell, B., Center for International
1600   Forestry Research, Bogor, Indonesia, 11–55 pp., 1996b.

Fuller, D. O.: Canopy phenology of some mopane and miombo woodlands in eastern Zambia, Global Ecology and Biogeography, 8, 199–209, https://doi.org/10.1046/j.1365-2699.1999.00130.x, 1999.

Fuller, D. O. and Prince, S. D.: Rainfall and foliar dynamics in tropical southern Africa: Potential impacts of global climatic change on Savanna vegetation, Clim Change, 33, 69–96, https://doi.org/10.1007/BF00140514, 1996a.

Fuller, D. O. and Prince, S. D.: Rainfall and foliar dynamics in tropical southern Africa: Potential impacts of global climatic change on Savanna vegetation, Clim Change, 33, 69–96, https://doi.org/10.1007/BF00140514, 1996b.

Funk, C., Peterson, P., Landsfeld, M., Pedreros, D., Verdin, J., Shukla, S., Husak, G., Rowland, J., Harrison, L., Hoell, A., and Michaelsen, J.: The climate hazards infrared precipitation with stations - A new environmental record for monitoring extremes, Sci Data, 2, 1–21, https://doi.org/10.1038/sdata.2015.66, 2015.

García, L., Rodríguez, J. D., Wijnen, M., and Pakulski, I.: Earth Observation for Water Resources Management: Current Use and Future Opportunities for the Water Sector, Washington, DC: World Bank, Washington, DC 20433, https://doi.org/10.1596/978-1-4648-0475-5, 2016.

Gates, D. M. and Hanks, R. J.: Plant factors affecting evapotranspiration, Irrigation of Agricultural Lands, 11, 506–521, https://doi.org/10.2134/agronmonogr11.c28, 2015.

Gerrits, A. M. J.: The role of interception in the ydrological cycle, PhD Thesis, Delft Univeristy of Technology, 146 pp., https://doi.org/http://resolver.tudelft.nl/uuid:7dd2523b-2169-4e7e-992c-365d2294d02e, 2010.

Ghysels, E., Osborn, D. R., and Rodrigues, P. M. M.: Chapter 13 Forecasting Seasonal Time Series, https://doi.org/10.1016/S1574-0706(05)01013-X, 2006.

Gokmen, M., Vekerdy, Z., Verhoef, A., Verhoef, W., Batelaan, O., and van der Tol, C.: Integration of soil moisture in SEBS for improving evapotranspiration estimation under water stress conditions, Remote Sens Environ, 121, 261–274, https://doi.org/10.1016/j.rse.2012.02.003, 2012.

Gray, J., Sulla-Menashe, D., and Friedl, M. A.: MODIS Land Cover Dynamics (MCD12Q2) Product, User Guide Collection 6, 6, 8, 2019.

Guan, K., Wood, E. F., Medvigy, D., Kimball, John., Pan, Ming., Caylor, K. K., Sheffield, J., Xu, Xiangtao., and Jones, M. O.: Terrestrial hydrological controls on land surface phenology of African savannas and woodlands, J Geophys Res Biogeosci, 119, 1652–1669, https://doi.org/10.1002/2013JG002572, 2014a.

Guan, K., Wood, E. F., Medvigy, D., Kimball, John., Pan, Ming., Caylor, K. K., Sheffield, J., Xu, Xiangtao., and Jones, M. O.: Terrestrial hydrological controls on land surface phenology of African savannas and woodlands, J Geophys Res Biogeosci, 119, 1652–1669, https://doi.org/10.1002/2013JG002572, 2014b.

Han, J., Zhao, Y., Wang, J., Zhang, B., Zhu, Y., Jiang, S., and Wang, L.: Effects of different land use types on potential evapotranspiration in the Beijing-Tianjin-Hebei region, North China,

1640 Journal of Geographical Sciences, 29, 922–934, https://doi.org/10.1007/s11442-019-1637-7, 2019.

Helsel, D. R., Hirsch, R. M., Ryberg, K. R., Archfield, S. A., and Gilroy, E. J.: Statistical Methods in Water Resources Techniques and Methods 4 – A3, USGS Techniques and Methods, 2020.

1645 Hulsman, P., Winsemius, H. C., Michailovsky, C. I., Savenije, H. H. G., and Hrachowitz, M.: Using altimetry observations combined with GRACE to select parameter sets of a hydrological model in a data-scarce region, Hydrol Earth Syst Sci, 24, 3331–3359, https://doi.org/10.5194/hess-24-3331-2020, 2020.

Hulsman, P., Hrachowitz, M., and Savenije, H. H. G.: Improving the Representation of Long-
1650 Term Storage Variations With Conceptual Hydrological Models in Data-Scarce Regions, Water Resour Res, 57, https://doi.org/10.1029/2020WR028837, 2021.

Jeffers, J. N. R. and Boaler, S. B.: Ecology of a Miombo site, Lupa North Forest Reserve, Tanzania I. weather and plant growth, 1962-64, Journal of Ecology, 54, 447–463, https://doi.org/10.2307/2257961, 1966.

1655 Jiménez, C., Prigent, C., and Aires, F.: Toward an estimation of global land surface heat fluxes from multisatellite observations, Journal of Geophysical Research Atmospheres, 114, 1–22, https://doi.org/10.1029/2008JD011392, 2009.

Jiménez, C., Prigent, C., Mueller, B., Seneviratne, S. I., McCabe, M. F., Wood, E. F., Rossow, W. B., Balsamo, G., Betts, A. K., Dirmeyer, P. A., Fisher, J. B., Jung, M., Kanamitsu, M., Reichle, R.
1660 H., Reichstein, M., Rodell, M., Sheffield, J., Tu, K., and Wang, K.: Global intercomparison of 12 land surface heat flux estimates, Journal of Geophysical Research Atmospheres, 116, 1–27, https://doi.org/10.1029/2010JD014545, 2011.

Kleidon, A. and Heimann, M.: A method of determining rooting depth from a terrestrial biosphere model and its impacts on the global water and carbon cycle, Glob Chang Biol, 4, 275–
1665 286, https://doi.org/10.1046/j.1365-2486.1998.00152.x, 1998a.

Kleidon, A. and Heimann, M.: A method of determining rooting depth from a terrestrial biosphere model and its impacts on the global water and carbon cycle, Glob Chang Biol, 4, 275–286, https://doi.org/10.1046/j.1365-2486.1998.00152.x, 1998b.

Kleine, L., Tetzlaff, D., Smith, A., Dubbert, M., and Soulsby, C.: Modelling ecohydrological
1670 feedbacks in forest and grassland plots under a prolonged drought anomaly in Central Europe 2018–2020, Hydrol Process, 35, https://doi.org/10.1002/hyp.14325, 2021.

Kramer, K., Leinonen, I., and Loustau, D.: The importance of phenology for the evaluation of impact of climate change on growth of boreal, temperate and Mediterranean forests ecosystems: An overview, https://doi.org/10.1007/s004840000066, 2000.

1675   Liu, M. and Hu, D.: Response of wetland evapotranspiration to land use/cover change and climate change in Liaohe River Delta, China, Water (Switzerland), 11, https://doi.org/10.3390/w11050955, 2019.

Liu, W., Wang, L., Zhou, J., Li, Y., Sun, F., Fu, G., Li, X., and Sang, Y. F.: A worldwide evaluation of basin-scale evapotranspiration estimates against the water balance method, J
1680   Hydrol (Amst), 538, 82–95, https://doi.org/10.1016/j.jhydrol.2016.04.006, 2016.

Liu, X., Chen, F., Barlage, M., and Niyogi, D.: Implementing Dynamic Rooting Depth for Improved Simulation of Soil Moisture and Land Surface Feedbacks in Noah-MP-Crop, J Adv Model Earth Syst, 12, https://doi.org/10.1029/2019MS001786, 2020.

Lu, P., Yu, Q., Liu, J., and Lee, X.: Advance of tree-flowering dates in response to urban climate
1685   change, Agric For Meteorol, 138, 120–131, https://doi.org/10.1016/j.agrformet.2006.04.002, 2006.

Macharia, D., Fankhauser, K., Selker, J. S., Neff, J. C., and Thomas, E. A.: Validation and Intercomparison of Satellite-Based Rainfall Products over Africa with TAHMO In Situ Rainfall Observations, J Hydrometeorol, 23, 1131–1154, https://doi.org/10.1175/JHM-D-21-0161.1,
1690   2022.

Makapela, L.: Review and use of earth observations and remote sensing in water resource management in South Africa : report to the Water Research Commission, 135 pp., 2015.

Marchesini, V. A., Fernández, R. J., Reynolds, J. F., Sobrino, J. A., and Di Bella, C. M.: Changes in evapotranspiration and phenology as consequences of shrub removal in dry forests of central
1695   Argentina, Ecohydrology, 8, 1304–1311, https://doi.org/10.1002/eco.1583, 2015.

Martens, B., Miralles, D. G., Lievens, H., Van Der Schalie, R., De Jeu, R. A. M., Fernández-Prieto, D., Beck, H. E., Dorigo, W. A., and Verhoest, N. E. C.: GLEAM v3: Satellite-based land evaporation and root-zone soil moisture, Geosci Model Dev, 10, 1903–1925, https://doi.org/10.5194/gmd-10-1903-2017, 2017.

1700   Martins, J. P., Trigo, I., and Freitas, S. C. e: Copernicus Global Land Operations "Vegetation and Energy" "CGLOPS-1," Copernicus Global Land Operations, 1–93, https://doi.org/10.5281/zenodo.3938963.PU, 2020.

Miralles, D. G., De Jeu, R. A. M., Gash, J. H., Holmes, T. R. H., and Dolman, A. J.: Magnitude and variability of land evaporation and its components at the global scale, Hydrol Earth Syst Sci,
1705   15, 967–981, https://doi.org/10.5194/hess-15-967-2011, 2011.

Miralles, D. G., Brutsaert, W., Dolman, A. J., and Gash, J. H.: On the Use of the Term "Evapotranspiration," Water Resour Res, 56, https://doi.org/10.1029/2020WR028055, 2020.

Mittermeier, R. A., Mittermeier, C. G., Brooks, T. M., Pilgrim, J. D., Konstant, W. R., Da Fonseca, G. A. B., and Kormos, C.: Wilderness and biodiversity conservation, Proc Natl Acad
1710   Sci U S A, 100, 10309–10313, https://doi.org/10.1073/pnas.1732458100, 2003.

Mu, Q., Heinsch, F. A., Zhao, M., and Running, S. W.: Development of a global evapotranspiration algorithm based on MODIS and global meteorology data, Remote Sens Environ, 111, 519–536, https://doi.org/10.1016/j.rse.2007.04.015, 2007.

Mu, Q., Zhao, M., and Running, S. W.: Improvements to a MODIS global terrestrial evapotranspiration algorithm, Remote Sens Environ, 115, 1781–1800, https://doi.org/10.1016/j.rse.2011.02.019, 2011.

Myneni, R. , Knyazikhin, Y., and Park, T.: MODIS/Terra Leaf Area Index/FPAR 8-Day L4 Global 500m SIN Grid V061, https://doi.org/https://doi.org/10.5067/MODIS/MOD15A2H.061, 2021.

Nelson, M., Hill, T., Remus, W., and O'connor, M.: Time Series Forecasting Using Neural Networks: Should the Data be Deseasonalized First?, J Forecast, 18, 359–367, 1999.

Nord, E. A. and Lynch, J. P.: Plant phenology: A critical controller of soil resource acquisition, J Exp Bot, 60, 1927–1937, https://doi.org/10.1093/jxb/erp018, 2009.

Novick, K. A., Ficklin, D. L., Stoy, P. C., Williams, C. A., Bohrer, G., Oishi, A. C., Papuga, S. A., Blanken, P. D., Noormets, A., Sulman, B. N., Scott, R. L., Wang, L., and Phillips, R. P.: The increasing importance of atmospheric demand for ecosystem water and carbon fluxes, Nat Clim Chang, 6, 1023–1027, https://doi.org/10.1038/nclimate3114, 2016.

ORNL DAAC: MODIS and VIIRS Land Products Global Subsetting and Visualization Tool, Subset obtained for MCD12Q2 product at [-12:76252], [32.48406], time period: [31-12-2020] to [31-12-2021], and subset size: [4]_[4] km,ORNL DAAC, ORNL DAAC, Oak Ridge, Tennessee, USA , 2018.

Pelletier, J., Paquette, A., Mbindo, K., Zimba, N., Siampale, A., Chendauka, B., Siangulube, F., and Roberts, J. W.: Carbon sink despite large deforestation in African tropical dry forests (miombo woodlands), Environmental Research Letters, 13, https://doi.org/10.1088/1748-9326/aadc9a, 2018.

Pereira, C. C., Boaventura, M. G., Cornelissen, T., Nunes, Y. R. F., and de Castro, G. C.: What triggers phenological events in plants under seasonal environments? A study with phylogenetically related plant species in sympatry, Brazilian Journal of Biology, 84, https://doi.org/10.1590/1519-6984.257969, 2022.

Pieruschka, R., Huber, G., and Berry, J. A.: Control of transpiration by radiation, Proc Natl Acad Sci U S A, 107, 13372–13377, https://doi.org/10.1073/pnas.0913177107, 2010.

Roberts, J. M.: The role of forests in the hydrological cycle, in: Forests and forest plants, vol. III, 1–10, 2013.

Running, Steven W, Qiaozhen Mu, Maosheng Zhao, A. M.: User ' s Guide MODIS Global Terrestrial Evapotranspiration (ET) Product NASA Earth Observing System MODIS Land Algorithm (For Collection 6), 2019.

Ryan, C. M., Pritchard, R., McNicol, I., Owen, M., Fisher, J. A., and Lehmann, C.: Ecosystem services from southern African woodlands and their future under global change, Philosophical Transactions of the Royal Society B: Biological Sciences, 371, https://doi.org/10.1098/rstb.2015.0312, 2016.

1750

Santin-Janin, H., Garel, M., Chapuis, J. L., and Pontier, D.: Assessing the performance of NDVI as a proxy for plant biomass using non-linear models: A case study on the kerguelen archipelago, Polar Biol, 32, 861–871, https://doi.org/10.1007/s00300-009-0586-5, 2009.

Savenije, H. H. G.: The importance of interception and why we should delete the term evapotranspiration from our vocabulary, Hydrol Process, 18, 1507–1511, https://doi.org/10.1002/hyp.5563, 2004.

1755

Savenije, H. H. G.: HESS opinions "topography driven conceptual modelling (FLEX-Topo)," Hydrol Earth Syst Sci, 14, 2681–2692, https://doi.org/10.5194/hess-14-2681-2010, 2010.

Schwartz, M. D.: Phenology: An Integrative Environmental Science, Second Edi., edited by: Schwartz, M. D., Springer Netherlands, Dordrecht, 503–519 pp., https://doi.org/10.1007/978-94-007-6925-0_27, 2013.

1760

Senay, G. B., Bohms, S., Singh, R. K., Gowda, P. H., Velpuri, N. M., Alemu, H., and Verdin, J. P.: Operational Evapotranspiration Mapping Using Remote Sensing and Weather Datasets: A New Parameterization for the SSEB Approach, J Am Water Resour Assoc, 49, 577–591, https://doi.org/10.1111/jawr.12057, 2013a.

1765

Senay, G. B., Bohms, S., Singh, R. K., Gowda, P. H., Velpuri, N. M., Alemu, H., and Verdin, J. P.: Operational Evapotranspiration Mapping Using Remote Sensing and Weather Datasets: A New Parameterization for the SSEB Approach, J Am Water Resour Assoc, 49, 577–591, https://doi.org/10.1111/jawr.12057, 2013b.

1770 Shahidan, M. F., Salleh, E., and Mustafa, K. M. S.: Effects of tree canopies on solar radiation filtration in a tropical microclimatic environment, Sun, Wind and Architecture - The Proceedings of the 24th International Conference on Passive and Low Energy Architecture, PLEA 2007, 400–406, 2007.

Sheil, D.: Forests, atmospheric water and an uncertain future: the new biology of the global water cycle, For Ecosyst, 5, https://doi.org/10.1186/s40663-018-0138-y, 2018.

1775

Snyder, R. L. and Spano, D.: Phenology and Evapotranspiration, in: Phenology: An Integrative Environmental Science, edited by: Mark D. Schwartz, Milwaukee, 521–528, 2013a.

Snyder, R. L. and Spano, D.: Phenology and Evapotranspiration, in: Phenology: An Integrative Environmental Science, edited by: Mark D. Schwartz, Milwaukee, 521–528, 2013b.

1780 Stancalie, G. and Nert, A.: Possibilities of Deriving Crop Evapotranspiration from Satellite Data with the Integration with Other Sources of Information, Evapotranspiration - Remote Sensing and Modeling, https://doi.org/10.5772/23635, 2012.

Stckli, R., Rutishauser, T., Baker, I., Liniger, M. A., and Denning, A. S.: A global reanalysis of vegetation phenology, J Geophys Res Biogeosci, 116, 1–19, https://doi.org/10.1029/2010JG001545, 2011.

Tian, F., Wigneron, J. P., Ciais, P., Chave, J., Ogée, J., Peñuelas, J., Ræbild, A., Domec, J. C., Tong, X., Brandt, M., Mialon, A., Rodriguez-Fernandez, N., Tagesson, T., Al-Yaari, A., Kerr, Y., Chen, C., Myneni, R. B., Zhang, W., Ardö, J., and Fensholt, R.: Coupling of ecosystem-scale plant water storage and leaf phenology observed by satellite, Nat Ecol Evol, 2, 1428–1435, https://doi.org/10.1038/s41559-018-0630-3, 2018a.

Tian, F., Wigneron, J. P., Ciais, P., Chave, J., Ogée, J., Peñuelas, J., Ræbild, A., Domec, J. C., Tong, X., Brandt, M., Mialon, A., Rodriguez-Fernandez, N., Tagesson, T., Al-Yaari, A., Kerr, Y., Chen, C., Myneni, R. B., Zhang, W., Ardö, J., and Fensholt, R.: Coupling of ecosystem-scale plant water storage and leaf phenology observed by satellite, Nat Ecol Evol, 2, 1428–1435, https://doi.org/10.1038/s41559-018-0630-3, 2018b.

Tuzet, A. J.: Stomatal Conductance, Photosynthesis, and Transpiration, Modeling, in: Encyclopedia of Agrophysics. Encyclopedia of Earth Sciences Series, edited by: Gliński, J., Horabik, J., Lipiec, J., Dordrecht, 855–858, https://doi.org/10.1007/978-90-481-3585-1_213, 2011.

Urban, J., Ingwers, M. W., McGuire, M. A., and Teskey, R. O.: Increase in leaf temperature opens stomata and decouples net photosynthesis from stomatal conductance in Pinus taeda and Populus deltoides x nigra, J Exp Bot, 68, 1757–1767, https://doi.org/10.1093/jxb/erx052, 2017.

Vermote, E. and Wolfe, R.: MOD09GA MODIS/Terra Surface Reflectance Daily L2G Global 1kmand 500m SIN Grid V006, https://doi.org/10.5067/MODIS/MOD09GA.006, 2015.

Vinya, R., Malhi, Y., Brown, N. D., Fisher, J. B., Brodribb, T., and Aragão, L. E. O. C.: Seasonal changes in plant – water relations in fl uence patterns of leaf display in Miombo woodlands : evidence of water conservative strategies, 104–112, https://doi.org/10.1093/treephys/tpy062, 2018.

Wang, S., Fu, B. J., Gao, G. Y., Yao, X. L., and Zhou, J.: Soil moisture and evapotranspiration of different land cover types in the Loess Plateau, China, Hydrol Earth Syst Sci, 16, 2883–2892, https://doi.org/10.5194/hess-16-2883-2012, 2012.

Wang-Erlandsson, L., Bastiaanssen, W. G. M., Gao, H., Jägermeyr, J., Senay, G. B., Van Dijk, A. I. J. M., Guerschman, J. P., Keys, P. W., Gordon, L. J., and Savenije, H. H. G.: Global root zone storage capacity from satellite-based evaporation, Hydrology and Earth System Sciences Discussions, 2016, https://doi.org/10.5194/hess-2015-533, 2016.

Weerasinghe, I., Bastiaanssen, W., Mul, M., Jia, L., and Van Griensven, A.: Can we trust remote sensing evapotranspiration products over Africa, Hydrol Earth Syst Sci, 24, 1565–1586, https://doi.org/10.5194/hess-24-1565-2020, 2020a.

Weerasinghe, I., Bastiaanssen, W., Mul, M., Jia, L., and Van Griensven, A.: Can we trust remote sensing evapotranspiration products over Africa, Hydrol Earth Syst Sci, 24, 1565–1586, https://doi.org/10.5194/hess-24-1565-2020, 2020b.

Wehr, R., Commane, R., Munger, J. W., Barry Mcmanus, J., Nelson, D. D., Zahniser, M. S., Saleska, S. R., and Wofsy, S. C.: Dynamics of canopy stomatal conductance, transpiration, and evaporation in a temperate deciduous forest, validated by carbonyl sulfide uptake, Biogeosciences, 14, 389–401, https://doi.org/10.5194/bg-14-389-2017, 2017.

White, F.: The Vegetation of Africa; a descriptive memoir to accompany the UNESCO/AETFAT/UNSO vegetation map of Africa, UNESCO, Paris, pp 352 pp., 1983.

World Bank: A Multi-Sector Investment Opportunities Analysis, Washington, D.C., 2010.

Zhang, K., Kimball, J. S., and Running, S. W.: A review of remote sensing based actual evapotranspiration estimation, https://doi.org/10.1002/wat2.1168, 1 November 2016.

Zhang, X., Friedl, M. A., Schaaf, C. B., Strahler, A. H., Hodges, J. C. F., Gao, F., Reed, B. C., and Huete, A.: Monitoring vegetation phenology using MODIS, Remote Sens Environ, 84, 471–475, https://doi.org/10.1016/S0034-4257(02)00135-9, 2003.

Zhao, M., Peng, C., Xiang, W., Deng, X., Tian, D., Zhou, X., Yu, G., He, H., and Zhao, Z.: Plant phenological modeling and its application in global climate change research: Overview and future challenges, Environmental Reviews, 21, 1–14, https://doi.org/10.1139/er-2012-0036, 2013.

Zimba, H., Coenders, M., Hulsman, P., van de Giesen, N., and Savenije, H. H. G.: ZAMSECUR Project Field Data Mpika, https://doi.org/https://doi.org/10.4121/19372352.V2, 2022.

Zimba, H., Coenders-Gerrits, M., Banda, K., Schilperoort, B., Van De Giesen, N., Nyambe, I., and Savenije, H. H. G.: Phenophase-based comparison of field observations to satellite-based actual evaporation estimates of a natural woodland: Miombo woodland, southern Africa, Hydrol Earth Syst Sci, 27, 1695–1722, https://doi.org/10.5194/hess-27-1695-2023, 2023.